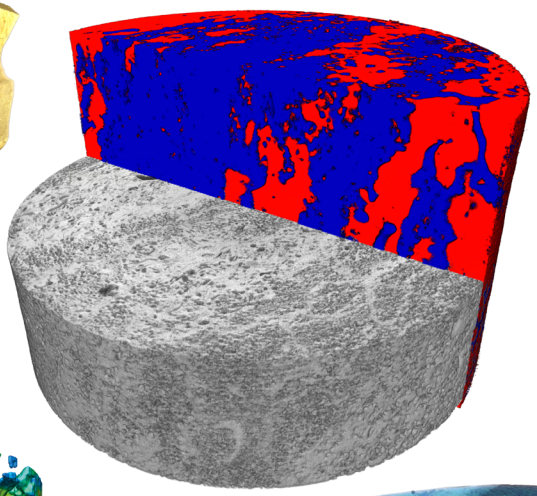

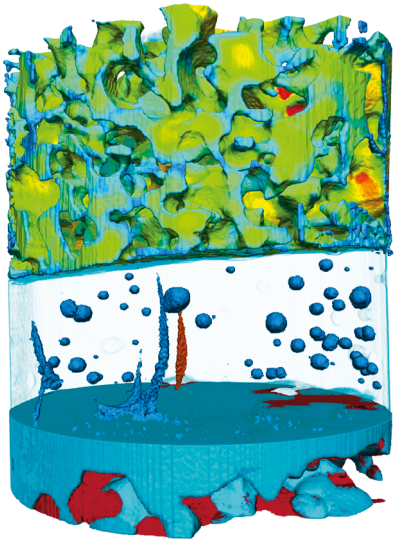

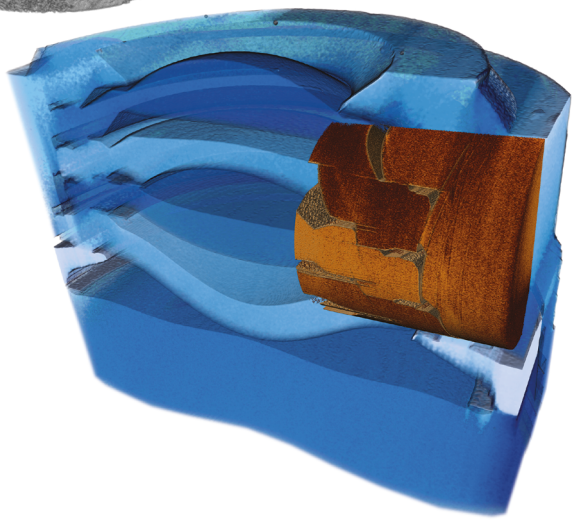

ZEISS X-ray Microscopes

A Reference List

ZEISS X-ray Microscopes
A Reference List

Author: *ZEISS Microscopy*
Pleasanton, California

Date: August 2018

Innovative 3D to 4D Imaging to Advance Science and Industry

From research to industry, ZEISS X-ray microscopes (XRM) are uniquely architected to facilitate quantitative understanding of microstructure under both ambient and *in situ* environmental conditions without destroying the sample. This enables imaging and tomography of microstructures as well as micro- and nano-structural evolution under a variety of conditions.

Our synchrotron heritage enabled us to develop superior lab-based XRM. The ZEISS Xradia Versa family, at true submicron spatial resolution 700 nm and minimum achievable voxel* size 70 nm, and the ZEISS Xradia Ultra family at 50 nm resolution and 16 nm voxel* are a new caliber of 3D X-ray microscope. These systems offer a distinct set of unique technological advantages beyond the limits of conventional micro- and nano-CT.

* *Voxel (sometimes referred to as "nominal resolution" or "detail detectability") is a geometric term that contributes to but does not determine resolution, and is provided here only for comparison. ZEISS specifies on spatial resolution, the most meaningful measurement of instrument resolution.*

What do ZEISS Xradia X-ray microscopes provide?

- Synchrotron Advancements to Laboratory – ongoing advancements and optical designs for 3D tomography are translated to the laboratory microscope systems for high resolution imaging, achieving spatial resolution down to 50nm
- Non-destructive Imaging – image the interior of a sample when physical sample cross-sectioning may cause undesirable, even unknown, damage to precious specimens
- 2D to 3D Datasets – XRM results are more than an image, but also a 3D quantitative dataset that can be used to complement computational models for iterative property-structure relationship analysis
- Superior Image Contrast – advanced synchrotron-based optics transferred to the laboratory system enable unparalleled phase contrast for low-Z (atomic number), low-density, and biological materials
- *In situ* to 4D Experiments – the ability to observe at high resolution the evolution of defects, such as cracks and voids, as a function of time and varying environmental conditions, by incorporating *in situ* experimental apparatuses

On the cover *(Clockwise from top left) Jaw of a black bear, segmented carbonate rock, mobile phone camera lens assembly, solid oxide fuel cell (SOFC). All samples imaged on ZEISS Xradia 520 Versa, except SOFC, imaged on ZEISS Xradia 810 Ultra.*

ZEISS Xradia Versa technology – Dual-stage optical architecture

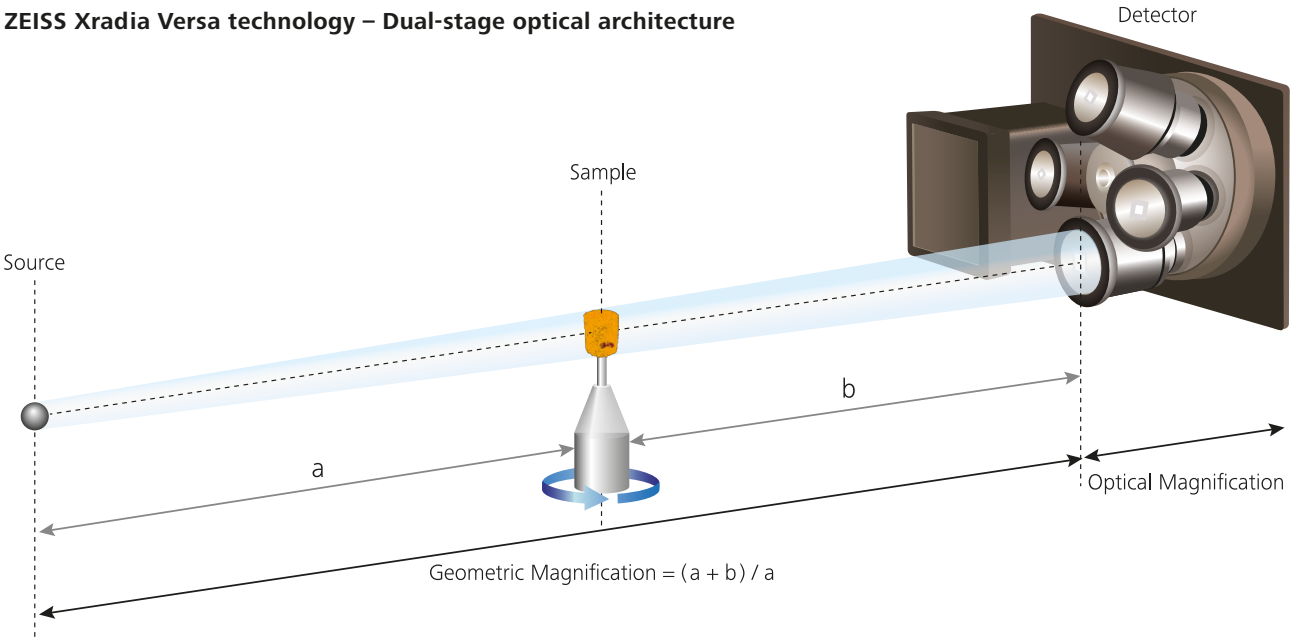

Xradia Versa architecture natively uses a two-stage magnification (geometric plus optical) technique to uniquely provide submicron resolution at large working distances, known as resolution at a distance (RaaD), for a large range of sample sizes.

ZEISS Xradia Ultra technology – Optical architecture

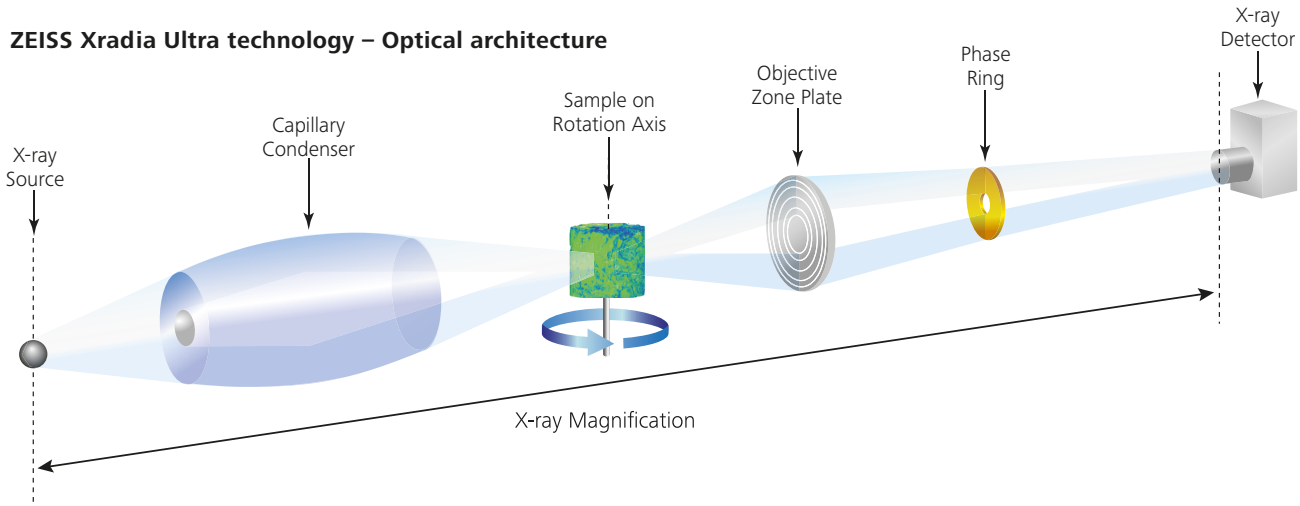

The architecture of Xradia Ultra is conceptually equivalent to an optical microscope or a transmission electron microscope (TEM). This architecture is also called transmission X-ray microscope, or TXM.

ZEISS Xradia X-ray Solutions

ZEISS Xradia 410 Versa
ZEISS Xradia 510 Versa
ZEISS Xradia 520 Versa

ZEISS Xradia 800 Ultra
ZEISS Xradia 810 Ultra

Global Scientific Impact of ZEISS X-ray Microscopes

ZEISS X-ray microscopy in the laboratory was born from developments in the synchrotron community over the past few decades. Synchrotron facilities across the world continue to push the limits of tomographic imaging in temporal, spatial, and energy resolution, and laboratory systems are now benefiting from this fertile "proving ground" for new detector and focusing optic technologies. This document provides a sample of hundreds of published research accounts from X-ray microscopy users around the world and their applications across diverse fields of research.

Peer-reviewed XRM Publications

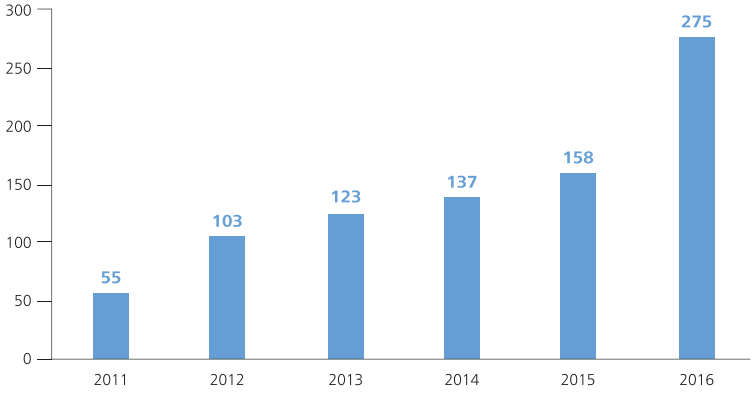

Source: Google Scholar (only publications where XRM model name is referenced are counted)

Where are they from? ZEISS Xradia X-ray microscopy authors publish from around the world.

Materials Science

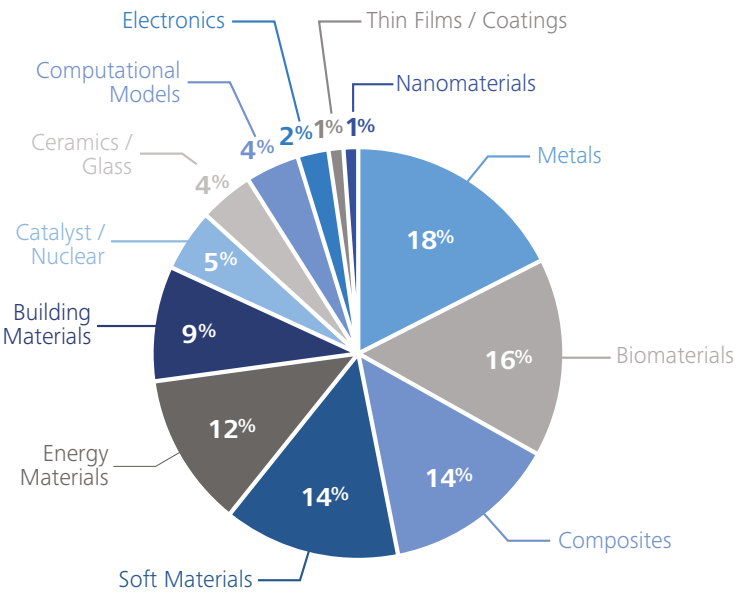

Life Sciences

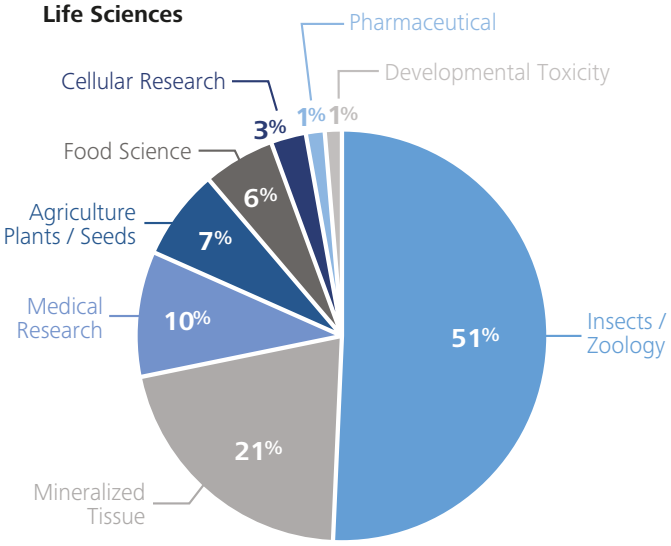

Geosciences

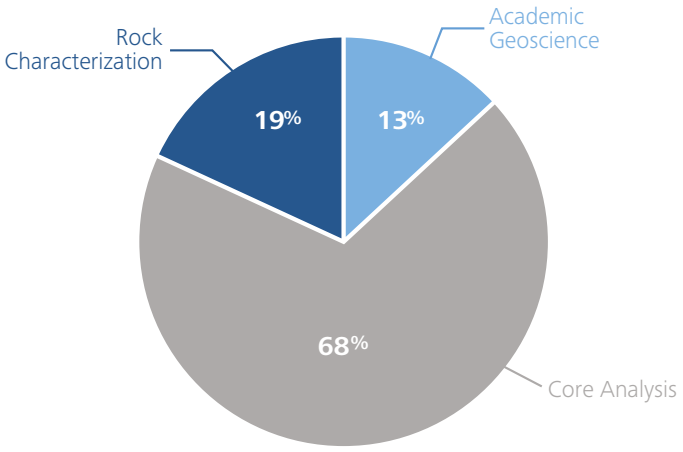

Peer-reviewed publications categorized by application for 2016 only.

Note: Publications using the ZEISS Ultra family are designated with "Ultra" label in the third column. The remainder were carried out using the ZEISS Versa family.

Materials Science

Energy Materials

Publications	Notes / Samples
Andisheh-Tadbir, M., Orfino, F. P., Kjeang, E. Three-dimensional phase segregation of micro-porous layers for fuel cells by nano-scale X-ray computed tomography. *J. Power Source*s 310, 61–69 (2016). DOI: 10.1016/j.jpowsour.2016.02.001	Fuel cell; micro-porous layer; carbon nanoparticle PTFE PEFC **Ultra**
Babu, S. K., Chung, H. T., Wu, G., Zelenay, P., Litster, S. Modeling Hierarchical Non-Precious Metal Catalyst Cathodes for PEFCs Using Multi-Scale X-ray CT Imaging. *ECS Trans.* 64, 281–292 (2014). DOI: 10.1149/06403.0281ecst	ZEISS Xradia 800 Ultra imaged PEFC section to its parameters. Then, generated model of sub-resolution features using XRM results as constraints PEFC **Ultra**
Babu, S. K., Litster, S. Vertically-Oriented Polymer Electrolyte Nanofiber Catalyst Support for Fuel Cells. *ECS Trans.* 58, 1137–1144 (2013). DOI: 10.1149/05801.1137ecst	Created track-etched polycarbonate structure, and used ZEISS Xradia 800 Ultra to characterize 3D pore geometries PEFC **Ultra**
Babu, S. K., Mohamed, A. I., Whitacre, J. F., Litster, S. Multiple imaging mode X-ray computed tomography for distinguishing active and inactive phases in lithium-ion battery cathodes. *J. Power Sources* 283, 314–319 (2015). DOI: 10.1016/j.jpowsour.2015.02.086	Li-ion battery cathode; imaged with both X-ray absorption and Zernike phase contrast to separate phases Batteries **Ultra**
Chen, Y., Zhang, Y., Lin, Y., Yang, Z., Su, D., Han, M., Chen, F. Direct-methane solid oxide fuel cells with hierarchically porous Ni-based anode deposited with nanocatalyst layer. *Nano Enaergy* (2014). DOI: 10.1016/j.nanoen.2014.08.016	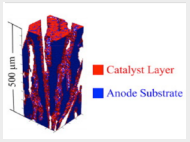 Thin nano samaria doped ceria (SDC) catalyst layer can effectively prevent coking. SOFC
Chung, D.-W., Shearing, P. R., Brandon, N. P., Harris, S. J., García, R. E. Particle Size Polydispersity in Li-Ion Batteries. *J. Electrochem. Soc.* 161, A422–A430 (2014). DOI: 10.1149/2.097403jes	LMO cathode imaged on ZEISS Xradia 410 Versa (formerly MicroXCT-400); results used to model microstructure and understand the effects of particle size distributions on electrochemistry Batteries
Eastwood, D. S., Bradley, R. S., Tariq, F., Cooper, S. J., Taiwo, O. O., Gelb, J., Merkle, A., Brett, D. J. L., Brandon, N. P., Withers, P. J., Lee, P. D., Shearing, P. R. The application of phase contrast X-ray techniques for imaging Li-ion battery electrodes. 324, 118-123, *Nucl. Instr. Meth. Phys. Res. B* (2014). DOI: 10.1016/j.nimb.2013.08.066	Laboratory ZEISS Xradia 800 Ultra (formerly nanoXCT-100) used to image a battery anode; first demonstration of Zernike phase contrast for imaging nano-scale features in a Li-battery Batteries **Ultra**
Eastwood, D. S., Yufit, F., Gelb, J., Gu, A., Bradley, R. S., Harris, S. J., Brett, D. J. L., Brandon, N. P., Lee, P. D., Withers, P. J., Shearing, P. R. Batteries: Lithiation-Induced Dilation Mapping in a Lithium-Ion Battery Electrode by 3D X-Ray Microscopy and Digital Volume Correlation, *Adv. Energy Mater.* 4, (2014). DOI: 10.1002/aenm.201470016	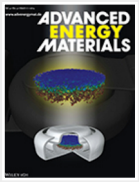 ZEISS Xradia Versa XRM system was used for repeated 3D imaging of an Li-battery in operand, allowing study of microstructural evolution in the working coin cell. Batteries
Epting, W. K., Gelb, J., Litster, S. Resolving the Three-Dimensional Microstructure of Polymer Electrolyte Fuel Cell Electrodes using Nanometer-Scale X-ray Computed Tomography. *Adv. Funct. Mater.* 22, 555–560 (2012). DOI: 10.1002/2Fadfm.201101525	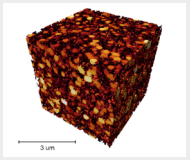 High-resolution (50 nm with ZEISS Xradia 800 Ultra), non-destructive imaging of the three-dimensional (3D) microstructures provides important new information on the size and form of the catalyst particle agglomerates and pore spaces PEFC **Ultra**
Epting, W. K., Litster, S. Effects of an agglomerate size distribution on the PEFC agglomerate model. *Int. J. Hydrogen Energy* 37, 8505–8511 (2012). DOI: 10.1016/j.ijhydene.2012.02.099	Nanoscale X-ray tomography microstructural data used for agglomerate size distribution PEFC **Ultra**

Materials Science

Energy Materials (continued)

Publications	Notes / Samples	
Finegan, D. P. et al. Characterising the structural properties of polymer separators for lithium-ion batteries in 3D using phase contrast X-ray microscopy. *Journal of Power Sources* 333, 184–192 (2016). DOI: 10.1016/j.jpowsour.2016.09.132	Phase contrast X-ray microscopy used to capture microstructures of commercial monolayer, tri-layer, and ceramic-coated lithium-ion battery polymer separator	Batteries **Ultra**
Garzon, F. H., Lau, S. H., Davey, J. R., Borup, R. Micro And Nano X-Ray Tomography of PEM Fuel Cell Membranes After Transient Operation. *ECS Trans.* 11, 1139–1149 (2007). DOI: 10.1149/1.2781026	XRM revealed a redistribution of Pt within the cathode, migration of Pt into the electrolyte membrane and significant amounts of carbon corrosion	PEFC
Gonzalez, J., Sun, K., Huang, M., Dillon, S., Chasiotis, I., Lambros, J. X-ray microtomography characterization of Sn particle evolution during lithiation/delithiation in lithium ion batteries. *J. Power Sources* 285, 205–209 (2015). DOI: 10.1016/2Fj.jpowsour.2015.03.093	Tin battery electrode imaged before and after the first charge cycle; quantified volumetric expansion of Sn-rich particles	Batteries
Gonzalez, J., Sun, K., Huang, M., Lambros, J., Dillon, S., Chasiotis, I. Three dimensional studies of particle failure in silicon based composite electrodes for lithium ion batteries. *J. Power Sources* 269, 334–343 (2014). DOI: 10.1016/j.jpowsour.2014.07.001	Microbattery cell built for testing in operando within the XRM; imaged silicon battery electrode before and after the first charge cycle; quantified volumetric expansion of Si-rich particles and bulk electrode	Batteries
Heenan, T. M. M., Brett, D. J. L. & Shearing, P. R. Mapping electrochemical activity in solid oxide fuel cells. *Materials Today* 20, 155–156 (2017). DOI: 10.1016/j.mattod.2017.03.015		SOFC **Ultra**
Izzo, J. R., Joshi, A. S., Grew, K. N., Chiu, W. K. S., Tkachuk, A., Wang, S. H., Yun, W. Nondestructive Reconstruction and Analysis of SOFC Anodes Using X-ray Computed Tomography at Sub-50 nm Resolution. *J. Electrochem. Soc.* 155, B504–B508 (2008). DOI: 10.1149/2F1.2895067	3D representation of microstructure is used to calculate true structural parameters; simulation of multicomponent mass transport and electrochemical reactions in the anode microstructure using the XRM data as geometric input illustrate the impact on SOFC modeling	SOFC **Ultra**
Jhong, H.-R. (Molly), Brushett, F. R., Yin, L., Stevenson, D. M., Kenis, P. J. A. Combining Structural and Electrochemical Analysis of Electrodes Using Micro-Computed Tomography and a Microfluidic Fuel Cell. *J. Electrochem. Soc.* 159, B292–B298 (2012). DOI: 10.1149/2.033203jes	XRM for detailed characterization of the architecture and buried interfaces of fuel cell electrodes in a non-destructive fashion	Fuel cell
Kehrwald, D., Shearing, P. R., Brandon, N. P., Sinha, P. K., Harris, S. J. Local Tortuosity Inhomogeneities in a Lithium Battery Composite Electrode. *J. Electrochem. Soc.* 158, A1393–A1399 (2011). DOI: 10.1149/2.079112jes	Generated ideal model for tortuosity and compared to XRM data; found significant local deviations in the tortuosity and estimated the impact on the battery charge/discharge behavior	Batteries **Ultra**
Khajeh-Hosseini-Dalasm, N., Sasabe, T., Tokumasu, T., Pasaogullari, U. Effects of polytetrafluoroethylene treatment and compression on gas diffusion layer microstructure using high-resolution X-ray computed tomography. *J. Power Sources* 266, 213–221 (2014). DOI: 10.1016/j.jpowsour.2014.05.004	*In situ* 3D compression study for heterogeneity in structure relative to fiber orientation; data is used for PEFC numerical transport models to include the effects of PTFE treatment and non-uniform compression	PEFC
Kinefuchi, I., Oyama, J., Yokoyama, K., Kubo, N., Tokumasu, T., Matsumoto, Y. Direct Simulation Monte Carlo Analysis of Gas Transport in Microporous Structure Based on X-ray Computed Tomography. *ECS Trans.* 58, 71–78 (2013). DOI: 10.1149/05801.0071ecst	Gas transport simulation based on XRM data	PEFC **Ultra**

Materials Science

Energy Materials (continued)

Publications	Notes / Samples
Kotaka, T., Aoki, O., Shiomi, T., Fukuyama, Y., Kubo, N., Tabuchi, Y. The Influence of Micro Structure of the GDL and MPL on the Mass Transport in PEFC. *ECS Trans.* 41, 439–448 (2011). DOI:10.1149/1.3635578	Diagnostics and phenomena - porous transport layers PEFC **Ultra**
Kotaka, T., Tabuchi, Y., Mukherjee, P. P. Microstructural analysis of mass transport phenomena in gas diffusion media for high current density operation in PEM fuel cells. *J. Power Sources* 280, 231–239 (2015). DOI: 10.1016/2Fj.jpowsour.2015.01.111	Structural data of gas diffusion media were obtained by XRM PEFC **Ultra**
Kumar, Arjun S., et al. Image segmentation of nanoscale Zernike phase contrast X-ray computed tomography images. *J. Appl. Phys.*117.18 (2015): 183102. DOI: 10.1063/1.4919835	Zernike phase contrast PEFC **Ultra**
Lim, C., Yan, B., Yin, L., Zhu, L. Simulation of diffusion-induced stress using reconstructed electrodes particle structures generated by micro/nano-CT. *Electrochimica Acta* 75, 279–287 (2012). DOI: 10.1016/j.electacta.2012.04.120	Imaged battery cathode and anode and generated a virtual model of the battery from the results; simulated volumetric expansions and quantified local stress induced as a result of expansion Batteries **Ultra**
Lim, C., Yan, B., Yin, L., Zhu, L. Geometric Characteristics of Three Dimensional Reconstructed Anode Electrodes of Lithium Ion Batteries. *Energies* 7, 2558–2572 (2014). DOI: 10.3390/en7042558	Quantified porosity, pore size distribution, and tortuosity; compared fresh anode versus cycled Batteries
Litster, S., Epting, W. K., Wargo, E. A., Kalidindi, S. R. Kumbur, E. C. Morphological Analyses of Polymer Electrolyte Fuel Cell Electrodes with Nano-Scale Computed Tomography Imaging. *Fuel Cells* 13, 935–945 (2013). DOI: 10.1002/fuce.201300008	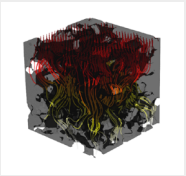 3D nano-CT data was analyzed according to several morphological characteristics, with particular focus on various effective pore diameters used in modeling gas diffusion in the Knudsen transition regime, which is prevalent in PEFC catalyst layers PEFC **Ultra**
Litster, S., Hess, K., Epting, W., Gelb, J. Catalyst Layer Analysis: Nanoscale X-ray CT, Spatially-Resolved *In Situ* Microscale Diagnostics, and Modeling. *ECS Trans.* 41, 409–418 (2011). DOI: 10.1149/1.3635575	Framework combines 50 nm resolution XRM, spatially-resolved *in situ* measurements with microstructured catalyst layer scaffold diagnostics, and porous electrode modeling PEFC **Ultra**
Mandal, P., Litster, S. Morphological Analysis of Polymer Electrolyte Fuel Cell Electrode Using High Resolution X-ray Computed Tomography and Subsequent Performance Analysis. *ECS Trans.* 58, 481–488 (2013). DOI: 10.1149/05801.0481ecst	GDE fabricated from the same catalyst layer slurry (ink) as the imaged samples were electrochemically evaluated in a PEFC PEFC
Odaya, S., Phillips, R.K., Sharma, Y., Bellerive, J., Phillion, A.B., Hoorfar, M. X-ray Tomographic Analysis of Porosity Distributions in Gas Diffusion Layers of Proton Exchange Membrane Fuel Cells. *Electrochimica Acta* 152, 464–472 (2015). DOI: 10.1016/j.electacta.2014.11.143	Proton exchange membrane fuel cell, gas diffusion layer, porosity, image analysis PEFC
Pattanotai, T., Watanabe, H., Okazaki, K. Effects of particle aspect ratio on pyrolysis and gasification of anisotropic wood cylinder. *Fuel* 150, 162–168 (2015). DOI: 10.1016/2Fj.fuel.2015.02.017	Visualized the 3D anisotropic structure of chars with various aspect ratios Other

Materials Science

Energy Materials (continued)

Publications	Notes / Samples
Paz-Garcia, J. M., Taiwo, O. O., Tudisco, E., Finegan, D. P., Shearing, P. R., Brett, D. J. L., Hall, S. A. 4D analysis of the microstructural evolution of Si-based electrodes during lithiation: Time-lapse X-ray imaging and digital volume correlation. *J. Power Sources* 320, 196–203 (2016). DOI: 10.1016/j.jpowsour.2016.04.076	Silicon battery at various states of charge; used digital volume correlation to map microstructure changes associated with lithiation delithiation Batteries
Pokhrel, A., El Hannach, M., Orfino, F. P., Dutta, M., Kjeang, E. Failure analysis of fuel cell electrodes using three-dimensional multi-length scale X-ray computed tomography. *J. Power Sources* 329, 330–338 (2016). DOI: 10.1016/j.jpowsour.2016.08.092	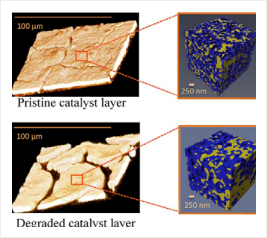 SOFC
Sasabe, T., Inoue, G., Tsushima, S., Hirai, S., Tokumasu, T., Pasaogullari, U. Investigation on Effect of PTFE Treatment on GDL Micro-structure by High-resolution X-ray CT. *ECS Trans.* 50, 735–744 (2013). DOI: 10.1149/05002.0735ecst	Micro-structure of the GDL was visualized by high-resolution X-ray computed tomography PEFC
Shearing, P. R., Brandon, N. P., Gelb, J., Bradley, R., Withers, P. J., Marquis, A. J., Cooper, S., Harris, S. J. Multi Length Scale Microstructural Investigations of a Commercially Available Li-Ion Battery Electrode. *J. Electrochem. Soc.* 159, A1023–A1027 (2012). DOI: 10.1149/2F2.053207jes	XRM survey: Versa XRM measured bulk structure and bulk porosity, Ultra XRM measured localized porosity, tortuosity, and volume-specific surface area, and Synchrotron XRM was needed for mapping defects within the particles Batteries **Versa Ultra**
Shearing, P. R., Gelb, J. Brandon, N. P. X-ray nano computerised tomography of SOFC electrodes using a focused ion beam sample-preparation technique. *Journal of the European Ceramic Society* 30, 1809–1814 (2010). DOI: 10.1016/j.jeurceramsoc.2010.02.004	Fuel cells, X-ray methods, microstructure, focused ion beam, SOFC SOFC
Song, R., Fang, R., Wen, L., Shi, Y., Wang, S., Li, F. A trilayer separator with dual function for high performance lithium–sulfur batteries. *J. Power Sources* 301, 179–186 (2016). DOI: 10.1016/j.jpowsour.2015.10.007	Battery separator in imaged in its "aged" state Batteries
Spernjak, D., Fairweather, J., Mukundan, R., Rockward, T., Borup, R. L. Influence of the microporous layer on carbon corrosion in the catalyst layerof a polymer electrolyte membrane fuel cell. *J. Power Sources* 214, 386–398 (2012). DOI: 10.1016/j.jpowsour.2012.04.086	PEM fuel cell, carbon corrosion, catalyst layer, microporous layer, current distribution, degradation mechanisms PEFC
Tjaden, B., Finegan, D. P., Lane, J., Brett, D. J. L. & Shearing, P. R. Contradictory concepts in tortuosity determination in porous media in electrochemical devices. *Chemical Engineering Science* 166, 235–245 (2017). DOI: 10.1016/j.ces.2017.03.051	Correlative tortuosity determinations via X-ray tomography and diffusion cell experiments **Ultra**
Tjaden, B. et al. The application of 3D imaging techniques, simulation and diffusion experiments to explore transport properties in porous oxygen transport membrane support materials. *Solid State Ionics* 288, 315–321 (2016). DOI: 10.1016/j.ssi.2016.01.030	Comparison of advanced tomography techniques, simulation and diffusion cell experiments to calculate tortuosity of a porous support layer of an oxygen transport membrane **Ultra**

Materials Science

Energy Materials

(continued)

Publications	Notes / Samples
Wargo, E. A., Kotaka, T., Tabuchi, Y., Kumbur, E. C. Comparison of focused ion beam versus nano-scale X-ray computed tomography for resolving 3-D microstructures of porous fuel cell materials. *J. Power Sources* 241, 608–618 (2013). DOI: 10.1016/j.jpowsour.2013.04.153	Focused ion beam, nanotomography, microstructure, polymer electrolyte fuel cell PEFC
Tariq, F., Kishimoto, M., Cooper, S. J., Shearing, P. R., Brandon, N. P. Advanced 3D Imaging and Analysis of SOFC Electrodes. *ECS Trans.* 57, 2553–2562 (2013). DOI: 10.1149/05701.2553ecst	Modeling and simulation SOFC
Yan, B., Lim, C., Yin, L., Zhu, L. Simulation of heat generation in a reconstructed LiCoO2 cathode during galvanostatic discharge. *Electrochimica Acta* 100, 171–179 (2013). DOI: 10.1016/j.electacta.2013.03.132	Battery electrode section was imaged and results were used to generate a model for simulating heat generation within the battery Batteries **Ultra**
Yan, B., Lim, C., Yin, L., Zhu, L. Three Dimensional Simulation of Galvanostatic Discharge of LiCoO2 Cathode Based on X-ray Nano-CT Images. *J. Electrochem. Soc.* 159, A1604–A1614 (2012). DOI: 10.1149/2F2.024210jes	Used nanoXCT-100 to image a battery and generate a model of the microstructure, which was used for simulating discharge behaviors. Batteries **Ultra**
Zhang, Y., Chen, Y., Chen, F. *In situ* quantification of solid oxide fuel cell electrode microstructure by electrochemical impedance spectroscopy. *J. Power Sources* 277, 277–285 (2015). DOI: 10.1016/j.jpowsour.2014.11.123	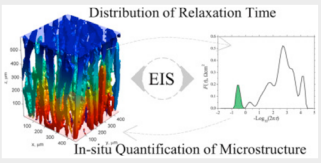 SOFC
Zhou, G., Pei, S., Li, L., Wang, D.-W., Wang, S., Huang, K., Yin, L.-C., Li, F., Cheng, H.-M. A Graphene-Pure-Sulfur Sandwich Structure for Ultrafast, Long-Life Lithium-Sulfur Batteries. *Adv. Mater.* 26, 625–631 (2014). DOI: 10.1002/adma.201302877	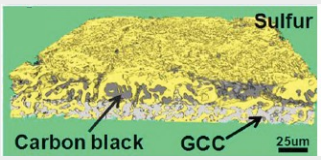 Batteries

Soft Materials & Biomaterials

Publication	Notes / Samples
Alderson, A., Alderson, K.L., McDonald, S.A., Mottershead, B., Nazare, S., Withers, P.J., Yao, Y.T. Piezomorphic Materials. *Macromol. Mater. Eng.* 298, 318–327 (2013). DOI: 10.1002/mame.201200028	Piezomorphic materials; ex-PTFE Polymer science
Balachander, G. M., Balaji, S. A., Rangarajan, A., Chatterjee, K. Enhanced Metastatic Potential in a 3D Tissue Scaffold toward a Comprehensive in Vitro Model for Breast Cancer Metastasis. *ACS Appl. Mater. Interfaces* 7, 27810–27822 (2015). DOI: 10.1021/acsami.5b09064	Breast cancer; cancer; mechanotransduction; metastasis; tissue scaffolds Tissue scaffold
Bosworth, L. A., Rathbone, S. R., Bradley, R. S., Cartmell, S. H. Dynamic loading of electrospun yarns guides mesenchymal stem cells towards a tendon lineage. *J. Mech. Behav. Biomed. Mater.* (2014). DOI: 10.1016/j.jmbbm.2014.07.009	Electrospun yarns; poly(ε-caprolactone) Biomaterials

Materials Science

Soft Materials & Biomaterials (continued)

Publication	Notes / Samples
Bradley, R. S. & Withers, P. J. Correlative multiscale tomography of biological materials. *MRS Bulletin* 41, 549–556 (2016). DOI: 10.1557/mrs.2016.137	Correlative tomography Biomaterials **Versa Ultra**
Bradley, R. S., Robinson, I. K. & Yusuf, M. 3D X-Ray Nanotomography of Cells Grown on Electrospun Scaffolds. *Macromol. Biosci.* 17, 2, (2017). DOI: 10.1002/mabi.201600236 *OPEN ACCESS*	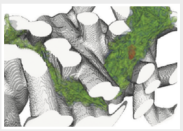 Zernike phase contrast can be used for 3D imaging of cells grown on electrospun polymer scaffolds Scaffolds **Ultra**
Caliari, S. R., Weisgerber, D. W., Grier, W. K., Mahmassani, Z., Boppart, M. D., Harley, B. A. C. Collagen Scaffolds Incorporating Coincident Gradations of Instructive Structural and Biochemical Cues for Osteotendinous Junction Engineering. *Adv. Healthcare Mater.* 4, 831 (2015). DOI: 10.1002/2Fadhm.201400809	Bone; collagen; mesenchymal stem cells; orthopedic interfaces; tendon Tissue scaffold
Ciecierska, E., Jurczyk-Kowalska, M., Bazarnik, P., Gloc, M., Kulesza, M., Kowalski, M., Krauze, S., Lewandowska, M. Flammability, mechanical properties and structure of rigid polyurethane foams with different types of carbon reinforcing materials. *Composite Structures* 140, 67–76 (2016). DOI: 10.1016/j.compstruct.2015.12.022	Foams; polyurethane; carbon nanotubes; graphite Foam
Costantini, M., Colosi, C., Mozetic, P., Jaroszewicz, J., Tosato, A., Rainer, A., Trombetta, M., Święszkowski, W., Dentini, M. Barbetta, A. Correlation between porous texture and cell seeding efficiency of gas foaming and microfluidic foaming scaffolds. *Mater. Sci. Eng.* C 62, 668–677 (2016). DOI: 10.1016/j.msec.2016.02.010	Microfluidic foaming; porous scaffolds; cell seeding efficiency; bioreactor Scaffolds
Costantini, M., Colosi, C., Jaroszewicz, J., Tosato, A., Święszkowski, W., Dentini, M., Garstecki, P., Barbetta, A. Microfluidic Foaming: A Powerful Tool for Tailoring the Morphological and Permeability Properties of Sponge-like Biopolymeric Scaffolds. *ACS Appl. Mater. Interfaces* 7, 23660–23671 (2015). DOI: 10.1021/acsami.5b08221	Alginate; microfluidic foaming; ordered porous structure; scaffolds Scaffolds
Divakaran, A. V., Torris A. T, A., Lele, A. K., Badiger, M. V. Porous PEG-PU hydrogels as potential biomaterials. *Polym. Int.* (2014). DOI:10.1002/pi.4802	Hydrogels; poly(ethylene glycol); polyurethane; porosity; permeability Hydrogels
Gergely, R. C. R., Pety, S.J., Krull, B.P., Patrick, J.F., Doan, T.Q., Coppola, A.M., Thakre, P.R., Sottos, N.R., Moore, J.S. Multidimensional Vascularized Polymers using Degradable Sacrificial Templates. *Adv. Funct. Mater.* (2014). DOI: 10.1002/adfm.201403670	Biopolymers; microfluidics; sacrificial templates; vascular Biopolymers
He, H., Zhong, M., Konkolewicz, D., Yacatto, K., Rappold, T., Sugar, G., David, N. E., Gelb, J., Kotwal, N., Merkle, A., Matyjaszewski, K. Three-Dimensionally Ordered Macroporous Polymeric Materials by Colloidal Crystal Templating for Reversible CO2 Capture. *Adv. Funct. Mater.* 23, 4720–4728 (2013). DOI: 10.1002/2Fadfm.201300401	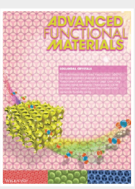 "…this demonstration showed the feasibility of using nanoscale 3D XRM for the visualization of the 3D morphology of 3DOM materials down to 50 nm resolution (16 nm voxels), representing up to three orders of magnitude improved resolution from the previous micro-CT experiments." CO_2 capture **Ultra**

Materials Science

Soft Materials & Biomaterials (continued)

Publication	Notes / Samples
Jang, H. L., Lee, K., Kang, C. S., Lee, H. K., Ahn, H.-Y., Jeong, H.-Y., Park, S., Kim, S. C., Jin, K., Park, J., Yang, T.-Y., Kim, J. H., Shin, S. A., Han, H. N., Oh, K. H., Lee, H.-Y., Lim, J., Hong, K. S., Snead, M. L., Xu, J. Nam, K. T. Biofunctionalized Ceramic with Self-Assembled Networks of Nanochannels. *ACS Nano* 9, 4447–4457 (2015). DOI: 10.1021/acsnano.5b01052	Bioinspired; ceramics; fluid transports; hierarchical structures; nanochannels; polymer agglomeration; pressure gradient sintering Biomaterials
Jackiewicz, A., Jakubiak, S. Gradoń, L. Analysis of the behavior of deposits in fibrous filters during non-steady state filtration using X-ray computed tomography. *Separation and Purification Technology* 156, 12–21 (2015). DOI: 10.1016/2Fj.seppur.2015.10.004	Fibrous filter; deep bed filtration; particle distribution; melt-blown Membrane
Jaroszewicz, J., Kosowska, A., Hutmacher, D., Swieszkowski, W. Moskalewski, S. Insight into characteristic features of cartilage growth plate as a physiological template for bone formation: CHARACTERISTIC FEATURES OF CARTILAGE GROWTH PLATE. *J. Biomed. Mater. Res. A* 104, 357–366 (2016). DOI: 10.1002/jbm.a.35575	Cartilage growth plate; 3D scaffold; mineralization; calcium deposits Bone scaffold
Jin, X., Shi, B., Zheng, L., Pei, X., Zhang, X., Sun, Z., … Jiang, L. Bio-Inspired Multifunctional Metallic Foams through the Fusion of Different Biological Solutions. *Advanced Functional Materials* 24(18), 2721–2726. (2014). DOI: 10.1002/adfm.201304184	Bio-inspired multifunctional metallic foams; surface engineering Biomaterials
Kijewska, K., Głowala, P., Kowalska, J., Jemielity, J., Kaczyńska, K., Janiszewska, K., Stolarski, J., Blanchard, G. J., Kępińska, D., Lubelska, K., Wiktorska, K., Pisarek, M. Mazur, M. Gold-decorated polymer vessel structures as carriers of mRNA cap analogs. *Polymer* 57, 77–87 (2015). DOI: 10.1016/2Fj.polymer.2014.12.019	Polypyrrole; polymer capsules Drug carriers
Kim, S. H., Shin, S.J., Lenhardt, J.M., Braun, T., Sain, J.D., Valdez, C.A., Leif, R.N., Kucheyev, S.O., Wu, K. J. J., Biener, J., Satcher Jr., J.H., Hamza, A.V. Deterministic Control over High-Z Doping of Polydicyclopentadiene-Based Aerogel Coatings. *ACS Appl. Mater. Interfaces* 5, 8111–8119 (2013). DOI: 10.1021/am4021878	Aerogels; dicyclopentadiene; ring-opening metathesis polymerization (ROMP) Aerogels
Kotoul, M. et al. Crack bridging modelling in Bioglass® based scaffolds reinforced by poly-vinyl alcohol/microfibrillated cellulose composite coating. *Mechanics of Materials* 110, 16–28 (2017). DOI: 10.1016/j.mechmat.2017.04.004	XRM data for 3D foam structure reconstruction; cell irregularities studied in connection to size effect and elastic properties Bioglass
Kumar, S., Azam, D., Raj, S., Kolanthai, E., Vasu, K. S., Sood, A. K. Chatterjee, K. 3D scaffold alters cellular response to graphene in a polymer composite for orthopedic applications: 3D SCAFFOLD ALTERS CELLULAR RESPONSE TO GRAPHENE. *J. Biomed. Mater. Res. Part B Appl. Biomater.* 104, 732–749 (2016). DOI: 10.1002/jbm.b.33549 *OPEN ACCESS*	Graphene-based polymer nanocomposites; scaffolds Scaffolds
Kumar, S. Chatterjee, K. Strontium Eluting Graphene Hybrid Nanoparticles Augment Osteogenesis in 3D Tissue Scaffold. *Nanoscale* (2014). DOI: 10.1039/C4NR05060F	Next generation of biomaterials for tissue regeneration Scaffold
Li, S. et al. Nanocomposites of graphene nanoplatelets in natural rubber: microstructure and mechanisms of reinforcement. *J. Mater. Sci.* 52, 9558–9572 (2017). DOI: 10.1007/s10853-017-1144-0	Characterization of nanocomposites of graphene nanoplatelets (GNPs) in natural rubber and bench-marked against nanocomposites loaded with N330 carbon black Rubber Graphene composites

Materials Science

Soft Materials & Biomaterials (continued)

Publication	Notes / Samples
Madani, A., Zeinoddini, S., Varahmi, S., Turnbull, H., Phillion, A.B., Olson, J. A., Martinez, D. M. Ultra-lightweight paper foams: processing and properties. *Cellulose* 1–9 (2014). DOI: 10.1007/s10570-014-0197-3	Cellulose fibres; papermaking; foam forming; lightweight materials Paper
Manickam, S. S., Gelb, J., McCutcheon, J. R. Pore structure characterization of asymmetric membranes: Non-destructive characterization of porosity and tortuosity. *J. Memb. Sci.* 454, 549–554 (2014). DOI: 10.1016/2Fj.memsci.2013.11.044	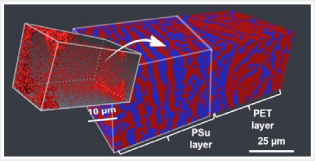 Membranes **Ultra**
Maiti, A. et al. 3D printed cellular solid outperforms traditional stochastic foam in long-term mechanical response. *Scientific Reports* 6, srep24871 (2016). DOI: 10.1038/srep24871 *OPEN ACCESS*	Foams imaged with X-ray computed tomography and carried out Finite-element analysis of stress distribution to aid anlaysis of long-term behavior 3D printing / Additive manufacturing
Meininger, S., Mandal, S., Kumar, A., Groll, J., Basu, B. Gbureck, U. Strength reliability and in vitro degradation of three-dimensional powder printed strontium-substituted magnesium phosphate scaffolds. *Acta Biomaterialia* 31, 401–411 (2016). DOI: 10.1016/j.actbio.2015.11.050	Magnesium phosphate; scaffold; strontium, 3D printing Scaffolds - bone
Mohan, N., Gupta, V., Sridharan, B., Sutherland, A., Detamore, M. S. The potential of encapsulating "raw materials" in 3D osteochondral gradient scaffolds. *Biotechnol. Bioeng.* 111(4), 829–841. (2014). DOI: 10.1002/bit.25145	Gradients in signals; raw materials; chondroitin sulfate; osteochondral tissue engineering; microsphere-based scaffold Scaffolds
Mural, P. K. S., Jain, S., Kumar, S., Madras, G. Bose, S. Unimpeded permeation of water through biocidal graphene oxide sheets anchored on to 3D porous polyolefinic membranes. *Nanoscale* 8, 8048–8057 (2016). DOI: 10.1039/C6NR01356B	Polyolefin based antibacterial 3D porous membranes for water purification Membrane
Naseri, N., Poirier, J.-M., Girandon, L., Fröhlich, M., Oksman, K. P. Mathew, A. 3-Dimensional porous nanocomposite scaffolds based on cellulose nanofibers for cartilage tissue engineering: tailoring of porosity and mechanical performance. *RSC Advances* 6, 5999–6007 (2016). DOI: 10.1039/c5ra27246g *OPEN ACCESS*	Porous scaffolds based on freeze-dried cellulose nanofibers Scaffolds - tissue
Nguyen, D. T., Kleiman, M., Ryu, K. A., Hiew, S., Brubaker, K., Mughnetsyan, R., Truong, R., Dolan, B., Tackett, E., Esser-Kahn, A. P. Three-Dimensional Conformal Coatings through the Entrapment of Polymer Membrane Precursors. *ACS Appl. Mater. Interfaces* (2014). DOI: 10.1021/am4053943	Coating; entrapment; microstructures; polymer membranes; three-dimensional Membrane
Ooi, C. H., Plackowski, C., Nguyen, A. V., Vadivelu, R. K., John, J. A. S., Dao, D. V. Nguyen, N.-T. Floating mechanism of a small liquid marble. *Scientific Reports* 6, 21777 (2016). DOI: 10.1038/srep21777 *OPEN ACCESS*	Liquid marble; surface science; contact angles of liquid-liquid interfaces Polymer science
Patterson, B. M., Henderson, K. Smith, Z. Measure of morphological and performance properties in polymeric silicone foams by X-ray tomography. *J. Mater. Sci.* 48, 1986–1996 (2013). DOI: 10.1007/s10853-012-6965-2	*In situ;* poly(dimethylsiloxane) (PDMS) foams Foam

Materials Science

Soft Materials & Biomaterials (continued)

Publication	Notes / Samples
Poologasundarampillai, G., Wang, D., Li, S., Nakamura, J., Bradley, R., Lee, P. D., Stevens, M. M., McPhail, D. S., Tasuga, T., Jones, J. R. Cotton-wool-like bioactive glasses for bone regeneration. *Acta Biomaterialia* (2014) DOI: 10.1016/j.actbio.2014.05.020 *OPEN ACCESS*	Electrospinning; sol–gel; bone regeneration scaffold; 3-D cotton-wool-like structure; inorganic fibers Bone scaffolds
Sai, H., Tan, K. W., Hur, K., Asenath-Smith, E., Hovden, R., Jiang, Y., Riccio, M., Muller, D. A., Elser, V., Estroff, L. A., Gruner, S. M., Wiesner, U. Hierarchical Porous Polymer Scaffolds from Block Copolymers. *Science* 341(6145), 530–534. (2013) DOI: 10.1126/science.1238159 *OPEN ACCESS*	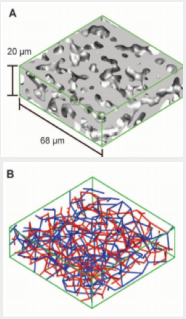 Macrostructure characterization and materials use as scaffold. (A) Isosurface visualization. (B) Skeletal networks for (A) of the polymeric (blue) and the porous (red) regions. Block copolymer scaffolds
Smolná, K., Gregor, T. Kosek, J. Morphological analysis of high-impact polypropylene using X-ray microCT and AFM. *Eur. Polym. J.* (2013). DOI: 10.1016/j.eurpolymj.2013.08.030	High-impact polypropylene particles; heterophase morphology Polymer science
Tsai, M.-C., Hung, K.-C., Hung, S.-C. Hsu, S. Evaluation of biodegradable elastic scaffolds made of anionic polyurethane for cartilage tissue engineering. *Colloids and Surfaces B: Biointerfaces* 125, 34–44 (2015). DOI: 10.1016/2Fj.colsurfb.2014.11.003	Biodegradable polyurethane; scaffold; elasticity; degradation; cartilage Scaffolds - tissue
Wen, L., Weaver, J. C., Lauder, G. V. Biomimetic shark skin: design, fabrication and hydrodynamic function. *The Journal of Experimental Biology* 217(10), 1656–1666, (2014). DOI: 10.1242/jeb.097097 *OPEN ACCESS*	 3D printing; biomimetic; hydrodynamics; shark skin; denticle; robot Biomemimetic
Wickramanayake, S., Hopkinson, D., Myers, C., Hong, L., Feng, J., Seol, Y., Plasynski, D., Zeh, M., Luebke, D. Mechanically robust hollow fiber supported ionic liquid membranes for CO2 separation applications. *J. Membrane Sci.* (2014) DOI: 10.1016/j.memsci.2014.07.015	Torlon; matrimid; hollow fiber; ionic liquid; strength Membrane
Wilts, B. D. et al. Butterfly gyroid nanostructures as a time-frozen glimpse of intracellular membrane development. *Science Advances* 3, e1603119 (2017). DOI: 10.1126%2Fsciadv.1603119	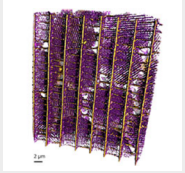 Biomaterials **Ultra**
Xia, Z., Villa, M. M., Wei, M. A biomimetic collagen–apatite scaffold with a multi-level lamellar structure for bone tissue engineering. *J. Mater. Chem. B* 2(14), 1998–2007. (2014). DOI: 10.1039/C3TB21595D	Biomimetic; scaffold; bone tissue engineering Bone scaffold

Materials Science

Metals

Publication	Notes / Samples
Barui, S., Chatterjee, S., Mandal, S., Kumar, A. & Basu, B. Microstructure and compression properties of 3D powder printed Ti-6Al-4V scaffolds with designed porosity: Experimental and computational analysis. *Materials Science and Engineering: C* 70, 812–823 (2017). DOI: 10.1016/j.msec.2016.09.040	XRM for intricate porosity assessment 3D printing/additive manufacturing
Bradley, R. s. et al. Time-lapse lab-based x-ray nano-CT study of corrosion damage. *Journal of Microscopy* 267, 98–106 (2017). DOI: 10.1111/jmi.12551	12-hour investigation of 3D corrosion damage AA2099 aluminum alloy Aluminum **Ultra**
Burnett, T.L., Holroyd, N.J.H., Lewandowski, J.J., Ogurreck, M., Rau, C., Kelley, R., Pickering, E.J., Daly, M., Sherry, A.H., Pawar, S., et al. Degradation of metallic materials studied by correlative tomography. *IOP Conf. Ser.: Mater. Sci. Eng.* 219, 012001 (2017). DOI: 10.1088/1757-899X/219/1/012001 *OPEN ACCESS*	Correlative tomography; multiscale and multi-instrument scheme **Versa** **Ultra**
Cao, Y. F., Chen, Y. Li, D. Z. Formation mechanism of channel segregation in carbon steels by inclusion flotation: X-ray microtomography characterization and multi-phase flow modeling. *Acta Materialia* 107, 325–336 (2016). DOI: 10.1016/j.actamat.2016.02.004	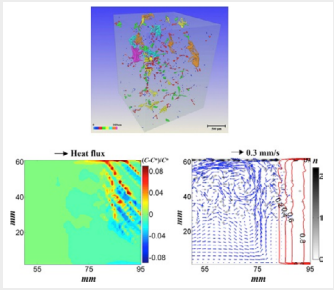 Steel
Cunsolo, S., Oliviero, M., Harris, W. M., Andreozzi, A., Bianco, N., Chiu, W. K. S., Naso, V. Monte Carlo determination of radiative properties of metal foams: Comparison between idealized and real cell structures. *International Journal of Thermal Sciences* 87, 94–102. (2015). DOI: 10.1016/j.ijthermalsci.2014.08.006	XRM can reveal the true foam structure, and provide a realistic computational domain and new insight for fluid and heat flow simulations Metal foam
Escobedo, J. P., Dennis-Koller, D., Cerreta, E. K., Patterson, B. M., Bronkhorst, C. A., Hansen, B. L., … Lebensohn, R. A. Effects of grain size and boundary structure on the dynamic tensile response of copper. *J. Appl. Phys.* 110(3), 033513–033513–13. (2011). DOI: 10.1063/1.3607294 *OPEN ACCESS*	Materials for extreme environments Copper
Fiedler, T., Sulong, M. A., Vesenjak, M., Higa, Y., Belova, I. V., Öchsner, A., Murch, G. E. Determination of the thermal conductivity of periodic APM foam models. *Int. J. Heat Mass Transfer* 73, 826–833. (2014). DOI: 10.1016/j.ijheatmasstransfer.2014.02.056	Cellular metal; advanced pore morphology foam; thermal conductivity; lattice Monte Carlo; analytical analysis Metal foam
Gamboa, E., Giuliani, M., Lavigne, O. X-ray microtomography observation of subsurface stress corrosion crack interactions in a pipeline low carbon steel. *Scripta Materialia* (2014). DOI: 10.1016/j.scriptamat.2014.01.038	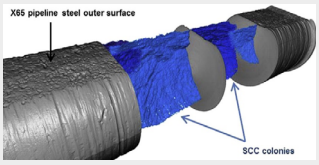 Steel
Gray, III, G. T., Bourne, N. K., Livescu, V., Trujillo, C. P., MacDonald, S., and Withers, P. The influence of shock-loading path on the spallation response of Ta. *Journal of Physics: Conference Series* 500(11), 112031. (2014) DOI: 10.1088/1742-6596/500/11/112031	Voids from the sample bulk Tantalum

Materials Science

Metals (continued)

Publication	Notes / Samples
Holesinger, T. G., Baca, F. J., Kennison, J. A., Coulter, J. Y., Patterson, B. M., Marken, K. R. Microstructure-Based Model for Current Flow in Bi-2212 Round Wire Conductors. *IEEE Transactions on Applied Superconductivity* 23(3), 6400305–6400305. (2013). DOI: 10.1109/TASC.2013.2238651	Critical current, microstructure, multifilamentary superconductors, superconducting materials Electrical
Iasiello, M., Cunsolo, S., Oliviero, M., Harris, W. M., Bianco, N., Chiu, W. K. S., Naso, V. Numerical Analysis of Heat Transfer and Pressure Drop in Metal Foams for Different Morphological Models. *Journal of Heat Transfer* 136(11), 112601–112601. (2014). DOI: 10.1115/1.4028113	XRM can revealed the true foam structure, and provided a realistic computational domain and new insight for fluid and heat flow simulations. Metal foam
Kim, S.-W., Hong, J. K., Na, Y.-S., Yeom, J.-T., Kim, S. E. Development of TiAl alloys with excellent mechanical properties and oxidation resistance. *Materials Design* (2013). DOI: 10.1016/j.matdes.2013.08.083	Intermetallic compounds; structural materials; electron microscopy; mechanical properties; microstructure turbine wheels Titanium
Knight, S. P., Salagaras, M., Trueman, A. R. The study of intergranular corrosion in aircraft aluminium alloys using X-ray tomography. *Corrosion Science* 53(2), 727–734. (2011). DOI: 10.1016/j.corsci.2010.11.005	XRM enabled visualization of IGC as well as characterization of corrosion growth direction, volume, depth, and width of intergranular fissure Aluminum
Leban, M. B., Tisu, R. The effect of TiN inclusions and deformation-induced martensite on the corrosion properties of AISI 321 stainless steel. *Engineering Failure Analysis* 33, 430–438. (2013). DOI: 10.1016/j.engfailanal.2013.06.021	Austenitic stainless steel; titanium nitride inclusions; deformation induced martensite; pitting corrosion; stress corrosion cracking Steel
Li, D., Chen, X.-Q., Fu, P., Ma, X., Liu, H., Chen, Y., Cao, Y., Luan, Y., Li, Y. Inclusion flotation-driven channel segregation in solidifying steels. *Nature Communication* (2014). DOI: 10.1038/ncomms6572 *OPEN ACCESS*	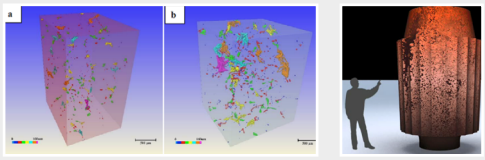 Steel
Li, X. P., O'Donnell, K. M. Sercombe, T. B. Selective laser melting of Al-12Si alloy: Enhanced densification via powder drying. *Additive Manufacturing* 10, 10–14 (2016). DOI: 10.1016/j.addma.2016.01.003	Selective laser melting; aluminium alloys 3D printing/additive manufacturing
Bacaicoa, I., Lütje, M., Sälzer, P., Umbach, C., Brückner-Foit, A., Heim, H.-P., Middendorf, B. Comparative investigation of two-dimensional imaging methods and X-ray tomography in the characterization of microstructure. *Materials Testing* 59, 829–836, (2017). DOI: 10.3139/120.111076	Dynamic image analysis, Al-Si-Cu-alloys, wood-plastic composites (WPC), foam concrete Aluminum
Ma, R., Wang, J., Yang, Z., Liu, M., Zhang, J., Jiang, L. Bioinspired Gas Bubble Spontaneous and Directional Transportation Effects in an Aqueous Medium. *Adv. Mater.*. 27, 2384, (2015). DOI: 10.1002/adma.201405087	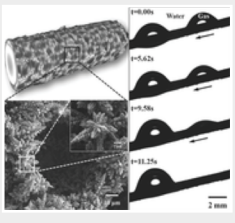 3D ordered gradient porous interconnected network surfaces of micro-nano hierarchical geometries constructed on a copper wire. Biomaterials-copper

Materials Science

Metals (continued)

Publication	Notes / Samples
Holzner, C., Lavery, Bale, H., Merklea, A., McDonald, S. Withers, P., Zhanga, Y. Juul Jensen, D. Kimura, K., Lyckegaard, A., Reischig, P. Lauridsena, E. M. Diffraction Contrast Tomography in the Laboratory – Applications and Future Directions. *Microscopy Today,* 24(04):34-43, July 2016. DOI: 10.1017/S1551929516000584	Diffraction contrast tomography **LabDCT**
McDonald, S.A., Holzner, C., Lauridsen, E.M., Reischig, P., Merkle, A.P., and Withers, P.J. Microstructural evolution during sintering of copper particles studied by laboratory diffraction contrast tomography (LabDCT). *Scientific Reports* 7, 5251, (2017). DOI: 10.1038/s41598-017-04742-1	Diffraction contrast tomography, 4D, sintering, copper powder **LabDCT**
McDonald, S.A., Reischig, P., Holzner, C., Lauridsen, E.M., Withers, P.J., Merkle, A.P., and Feser, M. Non-destructive mapping of grain orientations in 3D by laboratory X-ray microscopy. *Scientific Reports* 5, srep14665, (2015). DOI: 10.1038/srep14665	Diffraction contrast tomography, titanium **LabDCT**
Mostafavi, M., Bradley, R., Armstrong, D. E. J. & Marrow, T. J. Quantifying yield behaviour in metals by X-ray nanotomography. *Scientific Reports* 6, srep34346 (2016). DOI: 10.1038/srep34346 *OPEN ACCESS*	Study using digital volume correlation of X-ray nano-tomographs of a nanoindentation area to measure the sub-surface displacement field and plastic properties Steel strain **Ultra**
Patterson, B. M. et al. *In Situ* Laboratory-Based Transmission X-Ray Microscopy and Tomography of Material Deformation at the Nanoscale. *Exp Mech* 56, 1585–1597 (2016). DOI: 10.1007%2Fs11340-016-0197-3	Novel load stage for *in situ* mechanical testing enables both radiographic (2D) and tomographic (3D) characterization **Ultra**
Patterson, B. M., Escobedo-Diaz, J. P., Dennis-Koller, D., Cerreta, E. Dimensional Quantification of Embedded Voids or Objects in Three Dimensions Using X-Ray Tomography. *Microscopy and Microanalysis* 18(02), 390–398. (2012). DOI: 10.1017/S1431927611012554	3D quantification, copper spall, 3D statistics Copper
Patterson, B. M., Henderson, K. C., Gibbs, P. J., Imhoff, S. D. Clarke, A. J. Laboratory micro- and nanoscale X-ray tomographic investigation of Al–7 at%Cu solidification structures. *Materials Characterization* 95, 18–26 (2014). DOI: 10.1016/2Fj.matchar.2014.06.004	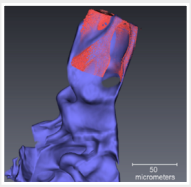 Overlay of Versa (blue) and Ultra (red) datasets. Ultra clearly resolves the eutectic structure. Copper-aluminum **Ultra**
Rao, A.G., Deshmukh, V.P., Lavery, L.L., Bale, H. 3D investigation of the microstructural modification in hypereutectic aluminum silicon (Al-30Si) alloy. *Microscopy & Analysis* 2017 www.microscopy-analysis.com/editorials/editorial-listings/3d-investigation-microstructural-modification-hypereutectic-aluminum	Phase-contrast imaging Aluminum-silicon
Slotwinski, J., Garboczi, E. J. Herbenstreit, K. Porosity Measurements and Analysis for Metal Additive Manufacturing Process Control. *J. Res. Natl. Inst. Stand. Technol.* 119, (2014). DOI: 10.6028/jres.119.019 *OPEN ACCESS*	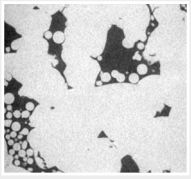 3D printing/additive manufacturing

Materials Science

Metals

(continued)

Publication	Notes / Samples
Sulong, M. A., Vesenjak, M., Belova, I. V., Murch, G. E., Fiedler, T. Compressive properties of Advanced Pore Morphology (APM) foam elements. *Mater. Sci. Eng. A* 607, 498–504. (2014). DOI: 10.1016/j.msea.2014.04.037	Finite element method; mechanical characterization aluminum alloys; plasticity Metal foam
Tammas-Williams, S., Withers, P. J., Todd, I. & Prangnell, P. B. Porosity regrowth during heat treatment of hot isostatically pressed additively manufactured titanium components. *Scripta Materialia* 122, 72–76 (2016). DOI: 10.1016/j.scriptamat.2016.05.002	Selective electron beam melting (SEBM), pores, heat treatment, hot isostatic pressing (HIPing) 3D printing/additive manufacturing
Topolski, K., Wieciński, P., Szulc, Z., Gałka, A., Garbacz, H. Progress in the characterization of explosively joined Ti/Ni bimetals. *Materials Design* 63, 479–487. (2014). DOI: 10.1016/j.matdes.2014.06.046	Explosive joining; bonding; titanium; nickel Bimetals
Wang, S., Wang, S., Zhang, L. Application of high resolution transmission X-ray tomography in material science. *Acta Metallurgica Sinica* 49(18), 897-910. (2013). DOI: 10.3724/SP.J.1037.2013.00107	Material science, metal, composites, *in situ* Tomography
Wu, Y., Liu, K., Su, B., Jiang, L. Superhydrophobicity-Mediated Electrochemical Reaction Along the Solid–Liquid–Gas Triphase Interface: Edge-Growth of Gold Architectures. *Adv. Mater.* 24(18), 2721–2726, (2013). DOI: 10.1002/adma.201304062	Superhydrophobicity, electrochemistry, micropillars, gold Surface engineering
Yu, Li, H. Y., Hardy, M. C., McDonald, S. A., Bowen, P. Mechanisms of dwell fatigue crack growth in an advanced nickel disc alloy RR1000. *MATEC Web of Conferences* 14, 6. (2014). DOI: 10.1051/matecconf/20141403002	SEM, ECCI and X-ray tomography have been adopted in the current study to understand the observed damage zone and retardation phenomenon. Superalloy
Yusuf, S. M., Chen, Y., Boardman, R., Yang, S. & Gao, N. Investigation on Porosity and Microhardness of 316L Stainless Steel Fabricated by Selective Laser Melting. *Metals* 7, 64 (2017). DOI: 10.3390/met7020064	Porosity; microhardness; Selective Laser Melting (SLM) 3D printing/additive manufacturing
Zhang, S. D., Zhang, W. L., Wang, S. G., Gu, X. J. Wang, J. Q. Characterisation of three-dimensional porosity in an Fe-based amorphous coating and its correlation with corrosion behaviour. *Corrosion Science* 93, 211–221 (2015). DOI: 10.1016/2Fj.corsci.2015.01.022	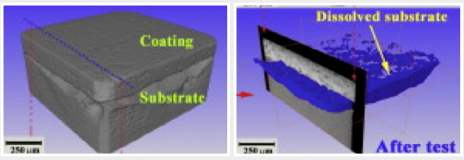 Corrosion

Nanomaterials

Publication	Notes / Samples
Du, X., Liu, H.-Y. Mai, Y.-W. Ultrafast Synthesis of Multifunctional N-Doped Graphene Foam in an Ethanol Flame. *ACS Nano* 10, 453–462 (2016). DOI: 10.1021/acsnano.5b05373	Graphene; electromechanical performance; compressibility Graphene
Jayanthi, S., Eswar, N. K., A. Singh, S., Chatterjee, K., Madras, G. K. Sood, A. Macroporous three-dimensional graphene oxide foams for dye adsorption and antibacterial applications. *RSC Advances* 6, 1231–1242 (2016). DOI: 10.1039/C5RA19925E	Graphene oxide; macroporous graphene foams; water remediation; anti-bacterial Study of 3D architecture of macroporous graphene foams, using X-ray microscopy and scanning electron microscopy Graphene

Materials Science

Nanomaterials

(continued)

Publication	Notes / Samples
Kim, J. H., Oh, S., Heo, Y.-U., Hata, S., Kumakura, H., Matsumoto, A., Mitsuhara, M., Choi, S., Shimada, Y., Maeda, M., MacManus-Driscoll, J. L. Dou, S. X. Microscopic role of carbon on MgB2 wire for critical current density comparable to NbTi. *NPG Asia Mater* 4, e3 (2012). DOI: 10.1038/2Fam.2012.3	Superconducting wire; MgB2; nanotomography, densification; Zernike phase contrast Superconductor **Ultra**
Li, Q. Effect of porosity and carbon composition on pore microstructure of magnesium/carbon nanotube composite foams. *Materials Design* 89, 978–987 (2016). DOI: 10.1016/j.matdes.2015.09.134	Pore microstructure of composite foams studied by X-ray microscopy. Porous magnesium composite; Carbon nanotubes; Porosity; x-ray micro-computed tomography Carbon nanotubes
Misak, H. E. Mall, S. Investigation into microstructure of carbon nanotube multi-yarn. *Carbon* 72, 321–327 (2014). DOI: 10.1016/j.carbon.2014.02.012	Carbon nanotube multi-yarn; X-ray nanotomography; phase contrast; FIB; SEM Carbon nanotubes
Stepanov, V., Willey, T. M., Ilavsky, J., Gelb, J. Qiu, H. Structural Characterization of RDX-Based Explosive Nanocomposites. *Propellants, Explosives, Pyrotechnics* 38, 386–393 (2013). http://dx.doi.org/10.1002%2Fprep.201200151	RDX-based nanocomposites; energetic materials; void and particle characterization by X-ray tomography Energetic materials **Ultra**

Ceramics / Glass

Publication	Notes / Samples
Cheng, S., Huang, H., Ovtar, S., Simonsen, S. B., Chen, M., Zhang, W., Søgaard, M., Kaiser, A., Vang Hendriksen, P., Chen, C. High-Performance Microchanneled Asymmetric $Gd_{0.1}Ce_{0.9}O_{1.95-\delta}$ – $La_{0.6}Sr_{0.4}FeO_{3-\delta}$ -Based Membranes for Oxygen Separation *ACS Appl. Mater. Interfaces*, 8 (7), 4548–4560, (2016). DOI: 10.1021/acsami.5b10714	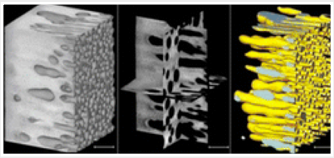 Dual phase composite membrane
Dong, L., Agnew, S., Wadley, H. Ni bonded TiC cermet pyramidal lattice structures *Extreme Mechanics Letters* 10, 2-14, (2017). DOI: 10.1016/j.eml.2016.11.004	Study of strut failure modes and correlation to micromechanics models Cermet
Jana, D.C., Sundararajan, G., Chattopadhyay, K. Effect of Porosity on Structure, Young's Modulus, and Thermal Conductivity of SiC Foams by Direct Foaming and Gelcasting, *J. Amer. Cer. Soc.,* 100 (1), 312-322, (2017) DOI: 10.1111/jace.14544	3D structural analysis: spherical pores with bimodal pore size distribution and changes in proportion of large size cell and interconnectivity Carbide Foams
Leo, A., Motuzas, J., Yacoua, C., Liu, S., Serrad, J.M., Navarrete, L., Drennan, J., Julbe, A., Diniz da Costa, J.C. Copper oxide - perovskite mixed matrix membranes delivering very high oxygen fluxes. *J. Mem. Sci.* 526, 323, (2017). DOI: 10.1016/j.memsci.2016.12.035	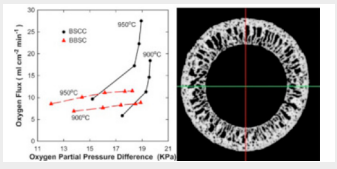 Membrane
Röding, M., Del Castillo, L.A., Nydén, M., Follink, B. Microstructure of a granular amorphous silica ceramic synthesized by spark plasma sintering *J. Microscopy* (2016) DOI: 10.1111/jmi.12442	By combining 2D and 3D imaging techniques with advanced statistical materials modelling, we reach deeper insight into the material structure and use. Plasma sintering

Materials Science

Ceramics / Glass

(continued)

Publication	Notes / Samples
Saucedo-Mora, L., Lowe, T., Zhao, S., Lee, P.D., Mummery, P.M., Marrow, T.J., *In situ* observation of mechanical damage within a SiC-SiC ceramic matrix composite *J. Nuclear Materials,* 481, 13, (2016). DOI: 10.1016/j.jnucmat.2016.09.007	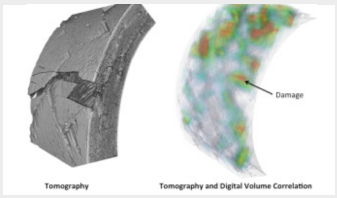 Ceramic matrix composite
Wu, Z., Sun, L., Wan, P., Li, J., Hu, Z. Wang, J. *In situ* foam-gelcasting fabrication and properties of highly porous γ-Y2Si2O7 ceramic with multiple pore structures. *Scripta Materialia* (2015). DOI: 10.1016/j.scriptamat.2015.02.024	Porous γ-Y2Si2O7 ceramic; microstructure; mechanical property; thermal conductivity Foam-gelcasting

Building Materials

Publication	Notes / Samples
Baniassadi, M., Safdari, M., Garmestani, H., Ahzi, S., Geubelle, P. H., Remond, Y. An optimum approximation of n-point correlation functions of random heterogeneous material systems. *J. Chem. Phys.* 140(7), 074905. (2014) DOI: 10.1063/1.4865966	Created a system of correlation functions to describe a highly varied material system; validated model against a real fibrous microstructure, as imaged by XRM Modeling
Bossa, N., Chaurand, P., Vicente, J., Borschneck, D., Levard, C., Aguerre-Chariol, O. Rose, J. Micro- and nano-X-ray computed-tomography: A step forward in the characterization of the pore network of a leached cement paste. *Cement and Concrete Research* 67, 138–147 (2015). DOI: 10.1016/2Fj.cemconres.2014.08.007	Used Versa & Ultra XRM to characterize leached-cement. Noted an increase in porosity in both cases, showed that nanoXCT provided increased image fidelity to capture the smaller details near the sample surface. Cement **Ultra Versa**
Cepuritis, R., Wigum, B. J., Garboczi, E. J., Mørtsell, E. Jacobsen, S. Filler from crushed aggregate for concrete: Pore structure, specific surface, particle shape and size distribution. *Cement and Concrete Composites* (2014). DOI: 10.1016/j.cemconcomp.2014.03.010	Used Versa to image concrete filler particles and compare to SEM results; compared particles on the basis of 3D shape. Concrete
Ducman, V., Korat, L., Legat, A. Mirtič, B. X-ray micro-tomography investigation of the foaming process in the system of waste glass–silica mud–MnO2. *Materials Characterization* 86, 316–321 (2013). DOI: 10.1016/j.matchar.2013.10.021	Compared particle porosities after different high-temperature thermal treatments using Versa XRM; Found that longer dwell times in heating lead to fewer – but larger – pores. Waste glass
Garcia, A., Austin, C. J. Jelfs, J. Mechanical properties of asphalt mixture containing sunflower oil capsules. *J. Cleaner Production* 118, 124–132 (2016). DOI: 10.1016/j.jclepro.2016.01.072	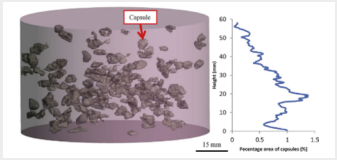 Self-healing asphalt
Wang, D., Wang, L., Gu, X., Zhou, G. Effect of Basalt Fiber on the Asphalt Binder and Mastic at Low Temperature. *J. Materials in Civil Engineering* 25(3), 355–364. (2013) DOI: 10.1061/(ASCE)MT.1943-5533.0000605	Examined structural properties of mastic (sealant) using Versa XRM. Used XRM resultsto generate a model for further simulation-based mechanical testing. Asphalt binder
Wicklein, B., Kocjan, A., Salazar-Alvarez, G., Carosio, F., Camino, G., Antonietti, M., Bergström, L. Thermally insulating and fire-retardant lightweight anisotropic foams based on nanocellulose and graphene oxide. *Nat Nano* 277–283 (2014). DOI: 10.1038/nnano.2014.248	nature nanotechnology Used Versa to characterize the pore geometries within a thermal insulation foam. Found that pores run parallel to the freezing direction and pore density at the bottom was similar to that at the top. Further analysis with SEM. Lightweight foams

Materials Science

Building Materials

(continued)

Publication	Notes / Samples
Zhang, M. Jivkov, A. P. Micromechanical modelling of deformation and fracture of hydrating cement paste using X-ray computed tomography characterisation. *Composites Part B: Engineering* 88, 64–72 (2016). DOI: 10.1016/j.compositesb.2015.11.007	Used Versa 410 to characterize the porosity in cement at various stages in the curing process. Focused on pore size distribution, where it was found that the pores get smaller with longer cure times. Cement paste
Zofka, A., Paliukaitė, M., Vaitkus, A., Maliszewska, D., Josen, R., Bernier, A. Laboratory study on the influence of casting on properties of ultra-high performance fibre reinforced concrete (UHPFRC) specimens. *J. Civil Engineering and Management* 20, 380–388 (2014). DOI: 10.3846/13923730.2014.913680	Used XRM to map the fiber orientation within a fiber reinforced concrete specimen. Found that one specimen exhibited random fiber orientations, while the other exhibited unfavorable fiber orientations. Fiber-reinforced concrete

Thin Films / Coatings

Publication	Notes / Samples
Ahmadian, S., Browning, A. & Jordan, E. H. Three-dimensional X-ray micro-computed tomography of cracks in a furnace cycled air plasma sprayed thermal barrier coating. *Scripta Materialia* 97, 13–16 (2015). DOI: 10.1016/j.scriptamat.2014.10.026	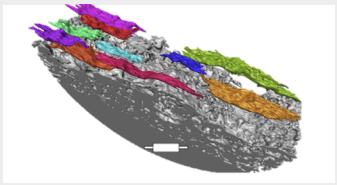 Thermal barrier coating
Cheng, S., Huang, H., Ovtar, S., Simonsen, S. B., Chen, M., Zhang, W., Søgaard, M., Kaiser, A., Hendriksen, P. V. Chen, C. High-Performance Microchanneled Asymmetric $Gd_{0.1}Ce_{0.9}O_{1.95-\delta}$ – $La_{0.6}Sr_{0.4}FeO_{3-\delta}$ -Based Membranes for Oxygen Separation *ACS Applied Materials Interfaces* 8, 4548–4560 (2016). DOI: 10.1021/acsami.5b10714	Dual-phase composite membranes; electrical conductivity relaxation; mass transfer polarization; phase inversion; surface exchange; thermodynamic calculation Dual phase composite membrane
Cordes, N. L., Havrilla, G. J., Usov, I. O., Obrey, K. A. Patterson, B. M. Non-destructive elemental quantification of polymer-embedded thin films using laboratory based X-ray techniques. *Spectrochimica Acta Part B: Atomic Spectroscopy* 101, 320–329 (2014). DOI: 10.1016/2Fj.sab.2014.09.016	Confocal micro-X-ray fluorescence; X-ray nanotomography; embedded thin films Polymer thin films
Niese, S. et al. Fabrication of Customizable Wedged Multilayer Laue Lenses by Adding a Stress Layer. *Thin Solid Films,* 571, 2, (2014). DOI:10.1016/j.tsf.2014.02.095	X-ray optics; diffractive optics; X-ray microscopy; multilayers; stress layer; sputter deposition Laue lenses

Catalyst / Nuclear

Publication	Notes / Samples
Bari, K., Osarinmwian, C., López-Honorato, E., Abram, T. J. Characterization of the porosity in TRISO coated fuel particles and its effect on the relative thermal diffusivity. *Nuclear Engineering and Design,* 265, 668–674, (2013). DOI: 10.1016/j.nucengdes.2013.08.067	Computed X-ray tomography at a resolution of 0.7 µm was used to quantify the porosity of each layer. TRISO
Chen, Y. et al. Direct-methane solid oxide fuel cells with hierarchically porous Ni-based anode deposited with nanocatalyst layer. *Nano Energy* 10, 1-9, (2014). DOI: 10.1016/j.nanoen.2014.08.016	Thin nano samaria doped ceria (SDC) catalyst layer can effectively prevent coking. Catalyst for fuel cell

Materials Science

Catalyst / Nuclear

(continued)

Publication	Notes / Samples
Cordes, N. L. et al. Three Dimensional Subsurface Elemental Identification of Minerals using Confocal Micro X-ray Fluorescence and Micro X-ray Computed Tomography. *Spectrochimica Acta Part B: Atomic Spectroscopy,* 103-104, 144-154, (2014). DOI:10.1016/j.sab.2014.12.006	Coupling of confocal X-ray fluorescence spectroscopy and X-ray computed tomography Confocal XRF
Ghiji, M., Goldsworthy, L., Brandner, P. A., Garaniya, V. Hield, P. Numerical and experimental investigation of early stage diesel sprays. *Fuel* 175, 274–286 (2016). DOI: 10.1016/j.fuel.2016.02.040	High-pressure diesel spray; primary atomization; near-nozzle flow; In-nozzle turbulence; large eddy simulation; Eulerian/VOF Nozzle flow
Giraldez, E. M. et al. Fabrication and Metrology Challenges in Making Thin, Hollow, Silver Spherical Halfraum Targets for EPEC Experiments on the National Ignition Facility. *Fusion Science and Technology* 63, 242–246 (2013). DOI: 10.13182/FST20-42	National Ignition Facility (NIF) Halfraum targets
Jhong, H.-R., Brushett, F. R. & Kenis, P. J. The Effects of Catalyst Layer Deposition Methodology on Electrode Performance. *Advanced Energy Materials,* 3, 589, (2013). DOI: 10.1002/aenm.201200759	Catalyst deposition;energy conversion and storage; microfluidic fuel cell; X-ray computed tomography; CO2 reduction Catalyst layer for fuel cell
Lowe, T. et al. Microstructural analysis of TRISO particles using multi-scale X-ray computed tomography. *J. Nuclear Materials* 461, 29–36 (2015). DOI:10.1016/j.jnucmat.2015.02.034	Multi-scale investigation of interior structure of TRISO particles TRISO **Versa** **Ultra**
Novák, V. et al. Effect of cavities and cracks on diffusivity in coated catalyst layer. *Catalysis Today* 216, 142–149 (2013). DOI: 10.1016/j.cattod.2013.07.002	Coating of commercial LNT monolith was scanned in 3D Catalyst coating
Pura, J. et al. Investigation of degradation mechanism of palladium–nickel wires during oxidation of ammonia. *Catalysis Today* 208, 48–55 (2013). DOI: 10.1016/j.cattod.2012.11.014	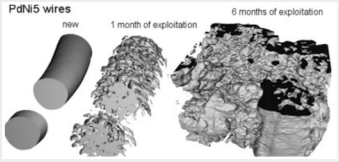 Precious metal; catalysis
Snead, L. L. et al. Stability of SiC-matrix microencapsulated fuel constituents at relevant LWR conditions. *J. Nuclear Materials* (2013). DOI: 10.1016/j.jnucmat.2013.09.056	Paper addresses certain key feasibility issues facing the application of SiC-matrix microencapsulated fuels for light water reactor application TRISO
Terrani, K. A. et al. Progress on matrix SiC processing and properties for fully ceramic microencapsulated fuel form. *J. Nuclear Materials* 457, 9–17 (2015). DOI: 10.1016/j.jnucmat.2014.10.034	X-ray radiographs of pellets were produced to examine the distribution of particles in the matrix Microencapsulated fuel form
Van Norman, S. A., Tringe, J. W., Sain, J. D., Yang, R., Falconer, J. L., Weimer, A. W. Using atomic layer deposited tungsten to increase thermal conductivity of a packed bed. *Appl. Phys. Lett.* 106, 153102 (2015). DOI: 10.1063/1.4917309	Understanding thermal properties of packed beds is essential for developing thermally conductive supports as alternatives to structured supports Catalysts

Materials Science

Electronics

Publication	Notes / Samples
Hattori, Y., Falgout, L., Lee, W., Jung, S.-Y., Poon, E., Lee, J. W., Rogers, J. A. Multifunctional Skin-Like Electronics for Quantitative, Clinical Monitoring of Cutaneous Wound Healing. *Advanced Healthcare Materials* 3(10), 1597–1607, (2014). DOI: 10.1002/adhm.201400073	Wound monitoring; clinical study; skin-like; multifunctional; epidermal electronics Wearable devices
Koh, A., Gutbrod, S. R., Meyers, J. D., Lu, C., Webb, R. C., Shin, G., Li, Y., Kang, S.-K., Huang, Y., Efimov, I. R. Rogers, J. A. Ultrathin Injectable Sensors of Temperature, Thermal Conductivity, and Heat Capacity for Cardiac Ablation Monitoring. *Advanced Healthcare Materials* 5, 373–381 (2016). DOI: 10.1002/adhm.201500451	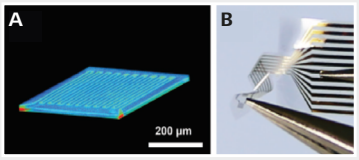 A) X-ray tomographic images of an actuator/sensor; B) picture of completed system in a twisted configuration Wearable devices
Kong, L., Rudack, A. C., Krueger, P., Zschech, E., Arkalgud, S. Diebold, A. C. 3D-interconnect: Visualization of extrusion and voids induced in copper-filled through-silicon vias (TSVs) at various temperatures using X-ray microscopy. *Microelectronic Engineering* 92, 24–28 (2012). DOI: 10.1016/2Fj.mee.2011.04.012	Through-silicon vias imaged by nanoscale X-ray tomography; void inspection; copper extrusion; defects; thermal stress TSV **Ultra**
Kong, L. W., Lloyd, J. R., Yeap, K. B., Zschech, E., Rudack, A., Liehr, M. Diebold, A. Applying x-ray microscopy and finite element modeling to identify the mechanism of stress-assisted void growth in through-silicon vias. *J. Applied Physics* 110, 53502-53502–7 (2011). DOI: 10.1063/2F1.3629988	4D annealing study of through-silicon vias (TSV) using nanoscale X-ray tomography TSV **Ultra**
Naman, O. T., New-Tolley, M. R., Lwin, R., Tuniz, A., Al-Janabi, A. H., Karatchevtseva, I., Fleming, S. C., Kuhlmey, B. T., Argyros, A. Indefinite Media Based on Wire Array Metamaterials for the THz and Mid-IR. *Advanced Optical Materials* 1(12), 971–977, (2013). DOI: 10.1002/adom.201300402	Metamaterials; indium wires with polymer coating Metamaterials
Niese, S., Krueger, P. Zschech, E. NanoXCT—A High- Resolution Technique For TSV Characterization. *AIP Conference Proceedings* 1378, 168–173 (2011). DOI: 10.1063/1.3615703	Lab-based non-desctructive XRM used to localize defects in copper TSVs for 3D IC integration. TSV **Ultra**
Schurch, R., Rowland, S. M., Bradley, R. S. Withers, P. J. Imaging and analysis techniques for electrical trees using X-ray computed tomography. *IEEE Transactions on Dielectrics and Electrical Insulation* 21, 53–63 (2014). DOI: 10.1109/TDEI.2013.003911	Degradation in polymeric high voltage insulation Electrical trees **Ultra**
Zhang, Y., Wang, S., Li, X., Fan, J. A., Xu, S., Song, Y. M., Choi, K, Yeo, W., Lee, W., Nazaar, S., Lu, B., Yin, L., Hwang, K., Rogers, J., Huang, Y. Experimental and Theoretical Studies of Serpentine Microstructures Bonded To Prestrained Elastomers for Stretchable Electronics. *Advanced Functional Materials* 24(14), 2028–2037, (2013). DOI: 10.1002/adfm.201302957	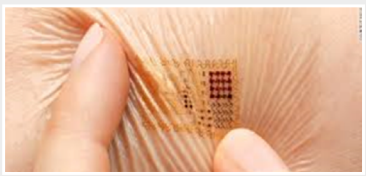 Flexible electronics
Zschech, E., Yun, W. Schneider, G. High-resolution X-ray imaging—a powerful nondestructive technique for applications in semiconductor industry. *Appl. Phys. A* 92, 423–429 (2008). DOI: 10.1007/s00339-008-4551-x	Failure analysis Semiconductor **Ultra**

Materials Science

Composites

Publication	Notes / Samples
Humeau, C., Davies, P. Jacquemin, F. Moisture diffusion under hydrostatic pressure in composites. *Materials Design* 96, 90–98 (2016). DOI: 10.1016/j.matdes.2016.02.012	X-ray micro-tomography is used and reveals a high level of porosity in the hand lay-up composite. Water diffusion
Islam, M. S. Tong, L. Influence of pinning on static strength of co-cured metal-GFRP hybrid single lap joints. *Composites Part A: Applied Science and Manufacturing* 84, 196–208 (2016). DOI: 10.1016/j.compositesa.2016.01.011	Hybrid, polymer-matrix composites (PMCs), mechanical testing, joints/joining PMC
O'Masta, M. R., Crayton, D. H., Deshpande, V. S. Wadley, H. N. G. Indentation of polyethylene laminates by a flat-bottomed cylindrical punch. *Composites Part A: Applied Science and Manufacturing* 80, 138–147 (2016). DOI: 10.1016/j.compositesa.2015.10.015	Laminates; polymer-matrix composites (PMCs); mechanical properties; mechanical testing PMC
Comer, A. J., Ray, D., Obande, W. O., Jones, D., Lyons, J., Rosca, I., O' Higgins, R. M., McCarthy, M. A. Mechanical characterisation of carbon fibre–PEEK manufactured by laser-assisted automated-tape-placement and autoclave. *Composites Part A: Applied Science and Manufacturing* 69, 10–20 (2015). DOI: 10.1016/2Fj.compositesa.2014.10.003	Automation; thermoplastic resin; carbon fibre; mechanical properties Carbon fiber
Gommer, F., Wedgwood, K. C. A. Brown, L. P. Stochastic reconstruction of filament paths in fibre bundles based on two-dimensional input data. *Composites Part A: Applied Science and Manufacturing* 76, 262–271 (2015). DOI: 10.1016/j.compositesa.2015.05.022	Carbon fibre ; microstructures ; analytical modelling; optical microscopy Carbon fiber
Yu, B., Bradley, R. S., Soutis, C., Hogg, P. J. Withers, P. J. 2D and 3D imaging of fatigue failure mechanisms of 3D woven composites. *Composites Part A: Applied Science and Manufacturing* 77, 37–49 (2015). DOI: 10.1016/j.compositesa.2015.06.013 *OPEN ACCESS*	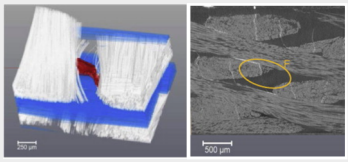 3D off-axis matrix cracking and virtual slice of debonding cracks Fiber, fatigue failure
Caty, O., Ibarroule, P., Herbreteau, M., Rebillat, R., Maire, E., Vignoles, G. L. Application of X-ray computed micro-tomography to the study of damage and oxidation kinetics of thermostructural composites. *Nuclear Instruments and Methods in Physics Research Section B: Beam Interactions with Materials and Atoms* 324, 113–117 (2014). DOI: 10.1016/j.nimb.2013.10.053	Damage; *in situ* tensile tests; oxidation ***in situ*** tests
Czabaj, M. W., Riccio, M. L. Whitacre, W. W. Numerical reconstruction of graphite/epoxy composite microstructure based on sub-micron resolution X-ray computed tomography. *Composites Science and Technology* 105, 174–182 (2014). DOI: 10.1016/j.compscitech.2014.10.017	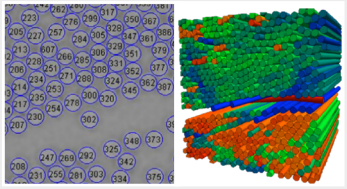 Graphite
Joffe, R., Madsen, B., Nättinen, Kalle, Miettinen, Arttu Strength of cellulosic fiber/starch acetate composites with variable fiber and plasticizer content. *Journal of Composite Materials,* 0021998314528734, (2014). DOI: 10.1177/0021998314528734	Cellulosic fibers, starch acetate, plasticizer, biocomposites, strength Cellulosic fiber

Materials Science

Composites (continued)

Publication	Notes / Samples
Joffre, T., Miettinen, A., Berthold, F. Kristofer Gamstedt, E. X-ray micro-computed tomography investigation of fibre length degradation during the processing steps of short-fibre composites. *Composites Science and Technology* (2014). DOI: 10.1016/j.compscitech.2014.10.011	Micro-structural parameters used in modeling of composite strength were obtained from optical observations and indirect measurements and some of these parameters were qualitatively verified by X-ray microtomography Short-fiber
Li, Q. Carbon nanotube reinforced porous magnesium composite: 3D nondestructive microstructure characterization using x-ray micro-computed tomography. *Materials Letters* 133, 83–86 (2014). DOI: 10.1016/j.matlet.2014.06.146	XRM was utilized to investigate 3D microstructure of porous magnesium composite reinforced by multi-walled carbon nanotubes and measure overall porosity Carbon nanotube
Patrick, J. F., Hart, K. R., Krull, B. P., Diesendruck, C. E., Moore, J. S., White, S. R., Sottos, N. R. Continuous Self-Healing Life Cycle in Vascularized Structural Composites. *Adv. Mater.* 26, 4302–4308 (2014). DOI: 10.1002/adma.201400248	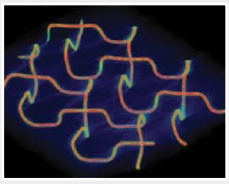 XRM used to visualize 3D microvascular channels to optimize incorporation into different composite layers Self-healing
Yoshimura, A., Hosoya, R., Koyanagi, J. Ogasawara, T. X-ray computed tomography used to measure fiber orientation in CFRP laminates. *Advanced Composite Materials* 0, 1–12 (2014). DOI: 10.1080/09243046.2014.959240	Measure the fiber orientation in CFRP laminates from XRM and digital image correlation (DIC) CRFP
Alemi-Ardakani, M., Milani, A. S., Yannacopoulos, S., Bichler, L., Trudel-Boucher, D., Shokouhi, G., Borazghi, H. Microtomographic Analysis of Impact Damage in FRP Composite Laminates: A Comparative Study. *Advances in Materials Science and Engineering,* 2013. DOI: 10.1155/2013/521860 *OPEN ACCESS*	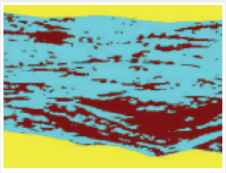 XRM reveals local failure modes and damage quantification for different structure types Laminates
Charnvanichborikarn, S., Shin, S. J., Worsley, M. A., Tran, I. C., Willey, T. M., van Buuren, T., Felter, T. E., Colvin, J. D., Kucheyev, S. O. Nanoporous Cu-C Composites Based on Carbon-Nanotube Aerogels. *J. Mater. Chem. A* (2013). DOI: 10.1039/C3TA14303A	XRM in 2D radiography Carbon nanotube aerogel
Chinga-Carrasco, G., Solheim, O., Lenes, M. Larsen, Å. A method for estimating the fibre length in fibre-PLA composites. *Journal of Microscopy* 250, 15–20 (2013). DOI: 10.1111/jmi.12012	Image analysis, pulp fibres, SEM, x-ray microtomography. Pulp fiber
Grabian, J., Gawdzińska, K., Wojnar, L. Przetakiewicz, W. An Application of Computer Tomography for Structure Characterization of Metallic-Ceramic Composite Foam. *Solid State Phenomena* 197, 226–231 (2013). DOI: 10.4028/www.scientific.net/SSP.197.226	Aluminum (Al), Metal-Ceramic Composites, Metallic Foam Metal-ceramic

Materials Science

Materials Microscopy

Publication	Notes / Samples	
Cordes, N. L. et al. Three Dimensional Subsurface Elemental Identification of Minerals using Confocal Micro X-ray Fluorescence and Micro X-ray Computed Tomography. *Spectrochimica Acta Part B: Atomic Spectroscopy,* 103-104, 144-154, (2014). DOI:10.1016/j.sab.2014.12.006	Coupling of confocal X-ray fluorescence spectroscopy and X-ray computed tomography	Confocal XRF
Rao, A.G., Deshmukh, V.P., Lavery, L.L., Bale, H. 3D investigation of the microstructural modification in hypereutectic aluminum silicon (Al-30Si) alloy. *Microscopy & Analysis* (2017) www.microscopy-analysis.com/editorials/editorial-listings/3d-investigation-microstructural-modification-hypereutectic-aluminum	Aluminum-silicon	Phase-contrast imaging
Bidola, P. et al. Application of sensitive, high-resolution imaging at a commercial lab-based X-ray micro-CT system using propagation-based phase retrieval. *Journal of Microscopy* 266, 211–220 (2017). DOI: 10.1111/jmi.12530	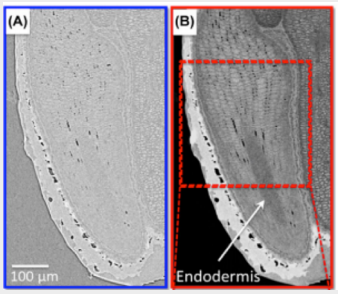	Phase-contrast imaging
Lavery, L., Merkle, A. Gelb, J. 3D X-ray Microscopy: A New High Resolution Tomographic Technology for Biological Specimens. *Microscopy and Microanalysis* 21, 925–926 (2015). DOI: 10.1017/S1431927615005425		XRM overview
Lavery, L. L., Gelb, J., Merkle, A. P. Steinbach, A. X-Ray Microscopy for Hierarchical Multi-Scale Materials. *Microscopy Today* 22, 16–21 (2014). DOI: 10.1017/S155192951400056X		XRM overview
Merkle, A. Automated correlative tomography using XRM and FIB-SEM to span length scales and modalities in 3D materials. *Microscopy Analysis* (2015). www.microscopy-analysis.com/magazine/issues/automated-correlative-tomography-using-xrm-and-fib-sem-span-length-scales-and		XRM overview

Materials Science

Art / Museum Materials

Publication	Notes / Samples
Howe, R., Shahbazmohamadi, S., Bass, R. Singh, P. Digital evaluation and replication of period wind instruments: the role of micro-computed tomography and additive manufacturing. *Early Music* cau091 (2014). DOI: 10.1093/em/cau091	XRM data used to replicate musical mouthpieces that no longer exist from methods like CNC milling and 3D printing/additive manufacturing. 3D printing Music
Marschallinger, R., Hofmann, P., Daxner-Höck, G. & Ketcham, R. A. Solid modeling of fossil small mammal teeth. *Computers & Geosciences* 37, 1364–1371 (2011). DOI: 10.1016/j.cageo.2010.07.011	XRM used to create digital models Fossil
Penney, D. et al. The Oldest Fossil Pirate Spider (Araneae: Mimetidae), in Uppermost Eocene Indian Amber, Imaged Using X-ray Computed Tomography. *Arachnology* 15, 299–302 (2012). DOI: 10.13156/arac.2012.15.9.299	Fossil
Urban, D. J. et al. Conjoined Twins in a Wild Bat: A Case Report. *Acta Chiropterologica* 17, 189–192 (2015). DOI: 10.3161/15081109ACC2015.17.1.016	Museum specimen

Geosciences

Publication	Notes / Samples
Jenniskens, P., Fries, M. D., Yin, Q.-Z., Zolensky, M., Krot, A. N., Sandford, S. A., Sears, D., Beauford, R., Ebel, D. S., Friedrich, J. M., Magashima, K., ... Worden, S. P. Radar-Enabled Recovery of the Sutter's Mill Meteorite, a Carbonaceous Chondrite Regolith Breccia. *Science,* 338(6114), 1583–1587, (2012). DOI: 10.1126/science.1227163	
Mungall, J. E., Brenan, J. M., Godel, B., Barnes, S. J. Gaillard, F. Transport of metals and sulphur in magmas by flotation of sulphide melt on vapour bubbles. *Nature Geosci* 8, 216–219 (2015). DOI: 10.1038/ngeo2373	
Popova, O. P., Jenniskens, P., Emel'yanenko, V., Kartashova, A., Biryukov, E., Khaibrakhmanov, S., Shuvalov, V., Rybnov, Y., Dudorov, A., ... Chelyabinsk, T. Airburst, Damage Assessment, Meteorite Recovery, and Characterization. *Science,* 342(6162), 1069–1073, (2013). DOI: 10.1126/science.1242642	
Lowrey, J.R., Ivanic, T.J., Wyman, D.A., Roberts, M.P. Platy pyroxene: new insights into spinifex texture. *Journal of Petrology,* egx069. DOI: 10.1093/petrology/egx069	

Cement

Publication	Notes / Samples
Pang, X., Maxson, J. K., Cuello Jimenez, W., Singh, J. P., Morgan, R. G. Microscale Characterization of Field and Laboratory Foamed Cement by Use of X-Ray Microcomputed Tomography. *Society of Petroleum Engineers* (October 2017). DOI:10.2118/180278-PA	

Coal

Publication	Notes / Samples
Shang, Y., Lebedev, M., Sarmadivaleh, M., Barifcani, A., Rahman, T., Iglauer, S. Swelling effect on coal micro structure and associated permeability reduction. *Fuel,* October 2016, Pages 568-576. DOI: 10.1016/j.fuel.2016.06.026	

Composites

Publication	Notes / Samples
Mathew, J., Mandal, A., WArnett, J., Williams, M.A., Chakraborty, M., Srirangam, P. X-ray tomography studies on porosity and particle size distribution in cast *in-situ* Al-Cu-TiB2 semi-solid forged composites. *Materials Characterization,* August 2016, Pages 57-64. DOI: 10.1016/j.matchar.2016.05.010	

Geosciences

Digital Rock Physics

Publication	Notes / Samples
Bai, B., ZHU, R., WU, S., YANG, W., Gelb, J., Gu, A., ZHANG, X. SU, L. Multi-scale method of Nano(Micro)-CT study on microscopic pore structure of tight sandstone of Yanchang Formation, Ordos Basin. *Petroleum Exploration and Development* 40, 354–358 (2013). DOI: 10.1016%2FS1876-3804(13)60042-7	**Ultra**
Dvorkin, J., Derzhi, N., Fang, Q., Nur, A., Nur, B., Grader, A., Baldwin, C., Tono, H. Diaz, E. From micro to reservoir scale: Permeability from digital experiments. *The Leading Edge* 28, 1446–1452 (2009). http://dx.doi.org/10.1190%2F1.3272699	**Ultra**
Katsevich, A., Frenkel, M., Feser, M., Huang, Z., Andrew, M., Case, T.,…Thompson, W. New Fast and Accurate 3D Micro Computed Tomography Technology for Digital Core Analysis. *Society of Petroleum Engineers* (2015, September 28). DOI:10.2118/174945-MS	
Saif, T., Lin, Q., Bijeljic, B., Blunt, M.J. Microstructural imaging and characterization of oil shale before and after pyrolysis. *Fuel,* June 2017, Pages 562-574. DOI: 10.1016/j.fuel.2017.02.030	
Semnani, S.J., Borja, R. I. Quantifying the heterogeneity of shale through statistical combination of imaging across scales. *Acta Geotechnica,* (2017). DOI: 10.1007/s11440-017-0576-7	
Shah, S.M., Gray, F., Crawshaw, J.P., Boek, E.S., Micro-computed tomography pore-scale study of flow in porous media: Effect of voxel resolution. *Advances in Water Resources,* September 2016, Pages 276-287. DOI: 10.1016/j.advwatres.2015.07.012	
Tölke, J., Baldwin, C., Mu, Y., Derzhi, N., Fang, Q., Grader, A., Dvorkin, J. Computer simulations of fluid flow in sediment: From images to permeability. *The Leading Edge* 29, 68–74 (2010). http://dx.doi.org/10.1190%2F1.3284055	**Ultra**
Wu, S., Zhu, R., Cui, J., Cui, J., Bai, B., Zhang, X., Jin, X., Zhu, D., You, J. Li, X. Characteristics of lacustrine shale porosity evolution, Triassic Chang 7 Member, Ordos Basin, NW China. *Petroleum Exploration and Development Online* 2, 185–195 (2015). DOI: 10.1016/2FS1876-3804(15)30005-7	**Ultra**
Zhou, M., Yang, J. Effect of the layer orientation on fracture propagation of Longmaxi Shale under uniaxial compression using micro-CT scanning. *SEG Technical Program Expanded Abstracts* 2017. August 2017, 3920-3924. DOI: 10.1190/segam2017-17654139.1	

Geosciences

Mining

Publication	Notes / Samples
Evans, C.L., Wightman, E.M., Yuan, X. Quantifying mineral grain size distributions for process modelling using X-ray micro-tomography. *Minerals Engineering,* October 2015, Pages 78-83. DOI: 10.1016/j.mineng.2015.03.026	

Multi-Phase Flow

Publication	Notes / Samples
Akbarabadi, M., Saraji, S., Piri, M., Georgi, D., Delshad, M. Nano-scale experimental investigation of *in-situ* wettability and spontaneous imbibition in ultra-tight reservoir rocks. *Advances in Water Resources* 107, 160–179 (2017). DOI: 10.1016/j.advwatres.2017.06.004	**Ultra**
Andrew, M., Bijeljic, B., Blunt, M.J. Pore-scale contact angle measurements at reservoir conditions using X-ray microtomography. *Advances in Water Resources,* June 2014, Pages 24-31. DOI: 10.1016/j.advwatres.2014.02.014	
Andrew, M., Bijeljic, B., Blunt, M.J. Pore-scale imaging of trapped supercritical carbon dioxide in sandstones and carbonates. *International Journal of Greenhouse Gas Control,* March 2014, Pages 1-14. DOI: 10.1016/j.ijggc.2013.12.018	
Andrew, M., Bijeljic, B., Blunt, M.J. Pore-by-pore capillary pressure measurements using X-ray microtomography at reservoir conditions: Curvature, snap-off, and remobilization of residual CO2. *Water Resour. Res.,* (2014). 50, 8760–8774. DOI: 10.1002/2014WR015970	
Menke, H.P., Bijeljic, B., Andrew, M. G., Blunt, M.J. Dynamic Three-Dimensional Pore-Scale Imaging of Reaction in a Carbonate at Reservoir Conditions. *Environmental Science & Technology* 2015 49 (7), 4407-4414. DOI: 10.1021/es505789f	
Ott, H., Andrew, M., Snippe, J., Blunt, M.J. Microscale solute transport and precipitation in complex rock during drying. *Geophys. Res. Lett.,* (2015). 41, 8369–8376. DOI: 10.1002/2014GL062266	
Scanziani, A., Singh, K., Blunt, M.J., Guadagnini, A. Automatic method for estimation of *in situ* effective contact angle from X-ray micro tomography images of two-phase flow in porous media. *Journal of Colloid and Interface Science,* June 2017, Pages 51-59. DOI: 10.1016/j.jcis.2017.02.005	
Tudek, J., Crandall, D., Fuchs, S., Werth, C.J., … Goodman, A. *In situ* contact angle measurements of liquid CO2, brine, and Mount Simon sandstone core using micro X-ray CT imaging, sessile drop, and Lattice Boltzmann modeling. *Journal of Petroleum Science and Engineering,* July 2017, Pages 3-10. DOI: 10.1016/j.petrol.2017.01.047	

Geosciences

Paleontology

Publication	Notes / Samples
Hickman-Lewis, K., Garwood, R.J., Withers, P.J., and Wacey. D. X-ray microtomography as a tool for investigating the petrological context of Precambrian cellular remains. *Geological Society,* London, Special Publications, 448, 33-56, 2 November 2016. DOI: 10.1144/SP448.11	
Park, T., Marx, F.G., Fitzgerald, E.M.G., Evans, A.R. The cochlea of the enigmatic pygmy right whale Caperea marginata informs mysticete phylogeny. *Journal of Morphology,* 2017; 278:801–809. DOI: 10.1002/jmor.20674	

X-ray Microscopy

Publication	Notes / Samples
Andrew, M., Graham, S., & Thompson, W. Iterative reconstruction techniques for X-ray microscopy in Geosciences. *Microscopy and Microanalysis,* (2017). 23(S1), 2162-2163. DOI:10.1017/S1431927617011473	

Carl Zeiss Microscopy GmbH
07745 Jena, Germany
microscopy@zeiss.com
www.zeiss.com/microscopy